Rapid whole brain 3D T 2 mapping respiratory-resolved Double-Echo Steady State (DESS) sequence with improved repeatability

Emile Kadalie, Aurélien Trotier, Nadège Corbin, Sylvain Miraux, Emeline Ribot

Rapid whole brain 3D T_2 mapping respiratory resolved DESS sequence with improved repeatability

Emile Kadalie[1], Aurélien J. Trotier[1], Nadège Corbin[1], Sylvain Miraux[1], Emeline J. Ribot[1]

[1]Centre de Résonance Magnétique des Systèmes Biologiques, UMR5536, CNRS/Université de Bordeaux, Bordeaux, France

Correspondence

Emeline J. Ribot, PhD, Centre de Résonance Magnétique des Systèmes Biologiques, 146 Rue Léo Saignat, 33076 Bordeaux, France. E-mail: emeline.ribot@rmsb.u-bordeaux.fr.

Manuscript Word Count: 5733

ABSTRACT

Purpose: To propose a quantitative 3D Dual Echo Steady State (DESS) sequence that offers rapid and repeatable T_2 mapping of the human brain using different encoding schemes that account for respiratory B_0 variation.

Methods: A retrospective self-gating module was firstly implemented into the standard DESS sequence in order to suppress the respiratory artifact via data binning. A Compressed-Sensing trajectory (CS-DESS) was then optimized to accelerate the acquisition. Finally, a spiral Cartesian encoding (SPICCS-DESS) was incorporated to further disrupt the coherent respiratory artifact. These different versions were compared to a standard DESS sequence (Fully DESS) by assessing the T_2 distribution and repeatability in different brain regions of eight volunteers at 3T.

Results: The respiratory artifact correction was determined to be optimal when the data was binned into 7 respiratory phases. Compared to the Fully DESS, T_2 distribution was improved for the CS-DESS and SPICCS-DESS with interquartile ranges reduced significantly by a factor ranging from 2 to 12 in the caudate, putamen and thalamus regions. In the gray and white matter areas, average absolute test-retest T_2 differences across all volunteers were respectively 3.5± 2% and 3.1±2.1% for the SPICCS-DESS, 4.6±4.6% and 4.9±5.1% for the CS-DESS, and 15%±13% and 7.3±5.6% for the Fully DESS. The SPICCS-DESS sequence's acquisition time could be reduced by half (< 4 min) whilst maintaining its efficient T_2 mapping.

Conclusion: The respiratory resolved SPICCS-DESS sequence offers rapid, robust and repeatable 3D T_2 mapping of the human brain, which can be especially effective for longitudinal monitoring of cerebral pathologies.

Keywords: DESS, T_2 mapping, respiratory B_0 variation, 3D brain imaging, qMRI

1. INTRODUCTION

The Dual Echo Steady State (DESS) sequence[1–3] has often been used in musculo-skeletal MRI to rapidly obtain high-contrast morphological images and quantitative T_2 mapping[4–8]. Two distinct steady-state free precession echoes, identified as $SSFP_{FID}$ and $SSFP_{Echo}$, are acquired and lead to the construction of two images with different contrasts. The ratio of both images is highly sensitive to the T_2 relaxation time[1] and can hence be used to procure T_2 maps. The possibility to estimate other quantitative parameters such as diffusion[9], B_0[10] and white matter myelin water content[11] has also been investigated with DESS-type sequences. Being a steady-state sequence, it employs short TRs which are especially practical for rapid 3D imaging. This offers a boost in signal-to-noise ratio (SNR), which is also improved by the use of low flip angles, an important asset for scans at high magnetic fields due to specific absorption rate concerns. Applications for knee imaging demonstrated accurate and precise T_2 estimates[4,12]. Recent studies have shown its potential in breast[13], prostate[14] and brain[15–17] imaging. This latter application is therefore an interesting prospect as T_2 mapping sequences can be used to monitor multiple cerebral pathologies including dementia[18], focal epilepsy[19], ischemia[20] and multiple or hippocampal sclerosis[21–23].

Nonetheless, the sequence has often been described as sensitive to physiological motion[13,15]. This sensitivity has been assumed to be the cause of artifacts as well as discrepancies in T_2 values, meaning that the reconstructed 3D T_2 maps are rapidly prone to deterioration and, therefore, misinterpretation. Previous work has noted the DESS sequence's particular sensitivity to B_0 fluctuation induced by respiration[24].

To avoid physiologically induced motion artifacts, retrospective self-gating[25], which allows the separation of data according to the subject's breathing or heartbeat after the MR acquisition, is of great interest when considering steady-state sequences such as the DESS. Avoiding triggering, and therefore interruptions in the acquisition, is vital in order to preserve the steady state of the magnetization. Multiple strategies can be employed, whether it be with physiological monitoring (ECG, respiratory belt)[26], or with the additional acquisition of a gating signal in the absence of phase encoding gradients[27]. While it has been shown to be a powerful tool for imaging the abdomen[28] and the heart[29], whether or not retrospective self-gating can be used to identify and correct such fluctuations efficiently on DESS brain images remains to be assessed.

Gating implies selecting the data according to the subjects' breathing in order to reconstruct time-resolved images, leading to either longer acquisition times or undersampled data. Compressed-Sensing[30,31] presents a set of advantages that accommodate such a compromise quite well. Not only does it provide high quality images with interesting acceleration factors but it also enables handling undersampled k-spaces adeptly with parallel imaging reconstruction as well as spatial and temporal regularizations[32,33].

Another way to circumvent artifacts caused by a periodic disruption of the encoding such as respiration is to change the manner in which the Cartesian phase encoding plane is sampled. Rather than traditionally acquiring the lines of k-space linearly along the phase and partition encoding directions, diversifying or randomizing the values of k_y and k_z at each repetition contains the potential to interrupt the respiratory coherence even further. The golden-step Cartesian trajectory with spiral profile ordering[34] samples the phase encoding plane in a spiral-like fashion, i.e., along spiral "interleaves" ordered according to a golden angle step. Such a technique represents an encoding scheme that could address the aforementioned problems without inducing other dilemmas such as Eddy currents resulting from drastic phase gradient changes.

Consequently, the overall objective of the current study was to implement rapid 3D DESS sequences that incorporated none, one, two or all of the previously mentioned techniques[25,30,34] (self-gating, Compressed-Sensing and spiral profile ordering) for brain imaging and to subsequently estimate their efficiency with respect to the respiratory correction as well as their T_2 estimates' repeatability.

2. METHODS

2.1. System

The experiments were performed on a 3T Prisma Siemens scanner using a body coil for transmission and a 64-channel head coil for signal reception.

2.2. Fully DESS sequence

An in-house Cartesian 3D DESS sequence was implemented. The $SSFP_{FID}$ and $SSFP_{Echo}$ images were acquired at echo times TE_1 and TE_2 respectively, where TE_2=TR-TE_1, with TR being the repetition time. Contrary to some previous works[12,14,15], an additional independent spoiler gradient was not implemented into the sequence in order to minimize the effects of diffusion on the T_2 mapping. This initial standard fully sampled version of the sequence will be consequently referred to as « Fully DESS ». A representative example showing a ghosting artifact on the images is available in Supporting Information Figure S1.

2.3. Self-Gating

In order to capture the influence of respiration on the DESS acquisitions, the additional acquisition of a gating signal at the start of every TR, was implemented (Figure 1a-b). This enabled the acquisition of 4 center k-space points which were then averaged. The resulting signal's phase captured the respiratory cycle and was therefore used retrospectively to sort the acquired k-space lines with respect

to their respiratory phase. For each respiratory phase, one volume could therefore be reconstructed. To avoid highly undersampled respiratory resolved volumes, multiple repetitions were performed. This adaptation will be designated as the « Gated DESS ».
The respiratory traces obtained with a respiratory belt on one participant during the acquisition were compared to the phase of the gating signal to confirm the correlation between them (see Supporting Information Figure S2).

2.4. Compressed-Sensing Trajectory

To shorten acquisition time, a Compressed-Sensing (CS) trajectory was then implemented with a variable density Poisson disk mask employed in the k_y-k_z plane ensuring a fully sampled center of 24x24 voxels (Figure 1c), subsequently used to estimate the coil sensitivity maps, and an acceleration factor of 8, as already described by Trotier et al[30]. To maximize the sampling of the k-space of each respiratory resolved volume, the undersampling mask was varied at each repeated acquisition, whilst maintaining the k-space center fully sampled. This accelerated version of the Gated DESS will be identified as the « CS-DESS » sequence.

2.5. Spiral Cartesian Trajectory

Once the Compressed-Sensing mask was applied, the encoding trajectory was further modified by implementing a golden-step Cartesian sampling with a spiral ordering in the phase encoded directions, inspired by the work of Prieto et al.[34]. This reordering could be adjusted according to the size of the spiral interleaf, i.e., the number of acquired lines from one end of a spiral to the other. In this case, the length of the spiral interleaf was set to the maximum, meaning that all the lines were encoded in a single spiral-like trajectory. This parameter was optimized in a preliminary study[35]. This version of the sequence, which incorporates Self-Gating, Compressed-Sensing, and a Spiral Cartesian trajectory, was named « SPICCS-DESS » thereafter (Spiral Cartesian Compressed-Sensing Dual Echo Steady-State) (Figure 1d).

2.6. Image Reconstruction

Reconstruction was achieved with the Gadgetron software[36] and the Berkeley Advanced Reconstruction Toolbox (BART, version 0.6)[37].
While the Fully DESS images were reconstructed with a classic inverse Fourier Transformation, the Gated DESS, CS-DESS and SPICCS-DESS volumes were handled differently. The gating signal was processed with the SSA-FARY method[38] after coil compression to 12 virtual coils (Figure 2). The principal components that best describe the respiratory oscillations, i.e., the first Empirical Orthonormal Functions (EOF) pair's phase portrait, were thus retrieved and divided into distinct bins,

i.e., separated according to their respiratory phases. The acquired k-data echoes could then be allocated to each of these bins and reorganized to construct a new k-space per bin. If more than one acquired echo could fill the same line in the k-space due to the repetitions, the echoes were averaged in order to maximize SNR. A low-resolution Gated DESS was first used to evaluate the optimal number of bins, from 1 to 10, and images were reconstructed for each bin with an inverse Fourier Transformation. The CS-DESS and SPICCS-DESS data were subsequently separated into 7 bins and images were consequently reconstructed from the resulting k-spaces by using joint parallel imaging and Compressed-Sensing[30] with spatial wavelet regularization (lambda=0.01), and temporal total variation regularization (lambda=0.5) along the bins, over 30 iterations. The resulting images from each bin were then summed up with a sum-of-squares for SNR enhancement.
To reduce the sequence's acquisition time, the SPICCS-DESS data was retrospectively reconstructed with NR=6 or 4 instead of 8 by omitting the last repetitions progressively 2 at a time.

2.7. T_2 mapping

The image ratio $SSFP_{Echo}/SSFP_{FID}$ was matched voxel-wise to a dictionary computed with the Extended Phase Graph algorithm[39–41] to perform T_2 mapping. The dictionary of signals obtained with the Sycomore toolkit[42] was built from the simulation of the DESS sequence for a given set of both fixed parameters (TR=15ms, TE_1=5ms, TE_2=10ms, Flip angle=10°, and Apparent Diffusion Coefficient=1 $\mu m^2/ms$ in order to approximate the diffusion effects of the readout gradients) and variable ones ($600<T_1<1600$ms incremented every 10ms, $70<B_1{}^+_{efficiency}<130\%$ incremented every 5%, $1<T_2<150$ms incremented every 1ms). Transverse magnetization states with populations inferior to a threshold of 0.01% of M_0 were considered to have negligible signal contributions and were ignored in order to save on computation time.
Voxel-wise T_1 (from a 3D Compressed-Sensing MP2RAGE sequence) and $B_1{}^+$ (2D PreSat-TFL B_1 sequence) values were directly obtained from the T_1 and $B_1{}^+$ maps, which were first co-registered to the DESS images using the SPM12 software (https://www.fil.ion.ucl.ac.uk/spm). (Figure 2).

2.8. Reconstruction analysis

The optimization and evaluation of the precision and repeatability of the methods were performed on the resulting T_2 maps using Matlab R2019b. For each subject, the segmentation of the coregistered MP2RAGE image was performed with SPM12[43]. Gray and white matter masks were defined by voxels for which the probability of belonging to the given tissue class exceeded 0.99. Volumetric brain information was also extracted from the MP2RAGE image using the volBrain software[44] allowing the analysis of multiple segmented brain structures (caudate, putamen, thalamus, pallidum, hippocampus).

2.9. In vivo experiments

The following in vivo experiments were conducted with approval granted by the local ethics committee and the informed written consent of the participants.

2.9.1. Optimization of the number of bins

Firstly, a low-resolution 3mm Gated DESS was acquired on a single subject in order to ascertain the effects of respiration on the images, evaluate the efficiency of the subsequent data binning and optimize the number of bins (respiratory cycle phases) to use for reconstruction. The parameters were: TR = 15 ms, TE_1 = 5 ms, TE_2 = 10 ms, flip angle = 10°, field of view (FOV) = 192 x 192 x 168 mm^3, matrix size = 64 x 64 x 56 (3mm isotropic resolution), Number of Repetitions (NR) = 50, Acquisition Time (TA) =44min51s, sagittal orientation, A >> P phase encoding direction, bandwidth = 390 Hz/pixel. NR=50 was necessary in order to ensure the complete filling of a maximum of 10 respiratory binned k-spaces and the ensuing inverse Fourier transform reconstruction.
The number of respiratory bins (Nbin) was varied from 1 to 10. For all Nbin, the standard deviation was computed in the background region of the 3D dataset reconstructed from a single bin. Additionally, the images were then compared to the one obtained with the maximum number of bins (Nbin=10) by computing the relative absolute difference. The mean signal from the entire dataset was measured for all resulting difference images. Finally, the standard deviation normalized by the mean of the estimated T_2 across the white matter region was investigated for all Nbin.

2.9.2. Application of the DESS methods

The following protocol was then carried out on eight healthy subjects (aged between 24 and 39 years, 3 females and 5 males).

The Fully DESS, CS-DESS and SPICCS-DESS sequences were performed twice (test-retest) after repositioning. The parameters were: TR = 15 ms, TE_1 = 5 ms, TE_2 = 10 ms, flip angle = 10°, FOV = 192 x 216 x 172.8 mm^3, matrix size = 160 x 180 x 144 (the FOV and matrix size were adapted to the head size of each volunteer while maintaining a 1.2mm isotropic resolution), TA=7min01s, sagittal orientation, A >> P phase encoding direction, bandwidth = 390 Hz/pixel. The CS-DESS and SPICCS-DESS were conducted with the acceleration parameters specified above and a number of repetitions (NR) set to 8, i.e., equal to the undersampling factor, in order to have acquisition times similar to the Fully DESS's. The NR was additionally set to 6 and 4 in retrospective reconstructions in order to evaluate the impact of reducing the number of repetitions on the method's performance.
A 3D Compressed-Sensing MP2RAGE sequence (MP2RAGE TR = 5000 ms, TI_1 = 800 ms, TI_2 = 2200 ms, TR = 7 ms, TE = 3.5 ms, flip angle = 7°, Echo Train Length = 125, FOV = 256 x 256 x 160 mm^3, matrix size = 256 x 256 x 160, 1mm isotropic resolution, TA=3 min 23 s, A >> P phase direction, bandwidth = 390 Hz/pixel, undersampling factor = 8) and a 2D PreSat-TFL B_1 mapping

sequence (TR = 16.45 s, TE = 1.92 ms, flip angle = 8°, FOV = 218 x 218 x 180 mm^3, matrix size = 128 x 128 x 25, TA=33 s, A >> P phase encoding direction, bandwidth = 490 Hz/pixel) were additionally acquired for each test and retest.

The impact of the number of bins was then estimated on the CS-DESS and SPICCS-DESS acquisitions by computing the associated k-space filling rates. This was calculated as the number of filled k-space lines divided by the total number of lines of a fully sampled k-space, i.e., the proportion of k-space that is sampled after the respiratory binning. This value was averaged for all subjects, and was calculated for a varying number of bins (5 to 9). The same operation was performed to calculate the filling rate of the k-space center, i.e., the sampled proportion of the 24 x 24 encoded lines in the center of k-space after the binning.

2.9.3. Analysis and validation

The CS-DESS and the SPICCS-DESS were compared to the Fully DESS by computing the T_2 values and their respective standard deviations across white and gray matter regions.

The distributions of T_2 values in those regions as well as in the caudate, putamen and thalamus regions were also measured with violin plots. Their interquartile ranges (IQR) of the three resulting groups (Fully, CS and SPICCS-DESS, with 8 subjects per group) were then compared via two right-sided Paired Student *t*-tests (Test 1: Fully vs CS, Test 2: CS vs SPICCS). Significant results ($P<0.01$) reflected a significantly higher IQR for the Fully than CS (Test 1) and a higher IQR for CS than SPICCS (Test 2).

The repeatability of the three sequences was assessed by means of Bland-Altman plots representing the voxel-wise T_2 differences between both tests normalized by their T_2 average, across all voxels of the white and gray matter regions and the three previously mentioned substructures, with respect to their T_2 average. The 95% confidence interval was computed by calculating the limits of agreement, i.e., the mean T_2 difference ± 1.96*standard deviation of the T_2 difference. The proportion of voxels in these regions with test-retest T_2 differences below 20% was also calculated, as well as *M*, the mean test-retest T_2 difference across all voxels in the caudate, putamen and thalamus regions.

Mathematically, $M = \mathrm{mean}(\{\mathrm{DIFF}_i\}_{1<i<N}) \pm \mathrm{std}(\{\mathrm{DIFF}_i\}_{1<i<N})$, where $\mathrm{DIFF}_i = \frac{v_{i,t}-v_{i,rt}}{\mathrm{mean}(v_{i,t},v_{i,rt})} \times 100$ represents the difference between the test-retest T_2 values $v_{i,t}$ and $v_{i,rt}$ of the *i*th voxel normalized by its average test-retest T_2 value and *N* is the total number of voxels in the selected structure. This was performed for each volunteer.

The tradeoff between the number of repetitions and the image quality of the SPICCS-DESS images was evaluated by assessing the T_2 distribution and repeatability in the different segmented regions of

the data retrospectively reconstructed with less repetitions. The T_2 interquartile ranges of the three groups (NR=8, NR=6 and NR=4) were evaluated with a left-sided Paired Student *t*-test (Test 1: NR=8 vs NR=6; Test 2: NR=6 vs NR=4).

3. RESULTS

3.1. Optimization of the number of bins

The Fully DESS images showed poor quality due to ghosting artifacts present in the sagittal direction, i.e., the partition encoding direction, despite the head being firmly set (Figure 3a, Figure 4a). These deteriorations were further amplified in the corresponding T_2 maps, particularly in the white matter region.

Applying the binning method in the 3mm Gated DESS reconstruction successfully mitigated the ghosting artifact (Figure 3). The noise i.e., the standard deviation in the affected background region, displayed a gradual decrease in the $SSFP_{FID}$ and $SSFP_{Echo}$ images as the number of bins increased, reaching a plateau towards 6-7 bins in the $SSFP_{Echo}$ image. The mean absolute signal difference between the reference image and the Gated DESS images demonstrated once more the progressive suppression of the artifact when increasing the number of bins. The white matter T_2 normalized standard deviation reached a plateau towards 7-8bins, decreasing from 38 to 26%. The Gated DESS protocol therefore confirmed that respiration was at the root of the image degradation and indicated that sorting the k-space lines into 7-8 bins of the respiratory cycle would be sufficient for optimal artifact correction.

Varying the number of bins from 5 to 9 demonstrated a progressive decrease in the CS-DESS and SPICCS-DESS filling rates (Table 1), from approximately 17.7% to 10.6% and from 82.6% to 60.2% for the k-space and k-space center, respectively. For 7 bins, the resulting k-spaces were filled approximately the same as a k-space with an undersampling factor of 8 (~13.4% filling rate) and around 70% of the k-space center was sampled, for all subjects. While a smaller number of bins resulted in a better filling rate, the metric measurements showed in Figure 3 indicated insufficient artifact correction. Conversely, a larger number of bins indicated a filling rate lower than that of a k-space with an undersampling factor of 8, and an artifact correction that did not largely improve with respect to the different metrics than the 7 bins reconstruction. This was the criterion that set 7 as the optimal number of respiratory bins used thereafter.

3.2. Analysis and validation

By following this approach, the artifact was largely suppressed in the CS-DESS and SPICCS-DESS images with 1.2mm voxel size when compared to the Fully DESS (Figure 4).
In the latter, T_2 values measured in the entire white matter region, for instance, were highly inhomogeneous for all subjects. In the representative case depicted in Figure 4, T_2 standard deviations were estimated to be 14.9ms and 23.8ms, i.e., 28% and 34% of the mean T_2 of the white and gray matter regions, respectively. For all the other subjects, they were measured to be between 23% and 47% in the white matter region and between 30 and 53% in the gray matter region, test and retest scans included.
The CS-DESS produced a notably more homogeneous T_2 map. In this case, T_2 standard deviations were reduced to 18% and 20% in the white and gray matter regions, respectively, in the representative case. For both test and retests of all volunteers, the standard deviation was also lower than with the Fully DESS and varied from 11 to 21% in the white matter and from 17 to 25% in the gray matter. However, it can be seen on the $SSFP_{Echo}$ in Figure 4 that the ghosting artifact was not completely suppressed, and the resulting T_2 map was asymmetrical with certain areas having lower T_2 values (highlighted by the dashed circle in the right hemisphere in Figure 4 for example).
In contrast, the SPICCS-DESS acquisition returned artifact-less anatomical images with the most homogeneous T_2 map. The T_2 standard deviations in the white matter region were reduced to 12% for the representative (17% in the gray matter region) and between 11 and 16% all volunteers/tests included (between 16 and 22% in the gray matter region).

Figure 5 further emphasizes the improvement of the T_2 mapping quality with the proposed protocol. The violin plots established a clear difference in the distribution of all voxels in the gray matter, white matter, caudate, putamen and thalamus regions between the Fully DESS and the accelerated DESS methods, for all subjects. The measured interquartile ranges were 2 to 12 times greater for the Fully DESS data. Indeed, in the Fully datasets, the IQR ranged between 25 and 32ms in the gray matter, between 15 and 27ms in the white matter, between 21 and 60ms in the caudate, between 14 and 64ms in the putamen and between 12 and 36ms in the thalamus, all volunteers included. On the contrary, the IQR in the CS-DESS datasets ranged between 12 and 16ms in the gray matter, between 7 and 10ms in the white matter, between 9 and 16ms in the caudate, between 6 and 11ms in the putamen and between 5 and 12ms in the thalamus. Finally, the IQR ranges in the SPICCS-DESS sequence were further reduced with ranges between 11 and 15ms in the gray matter, between 6 and 10ms in the white matter, between 8 and 12ms in the caudate, between 5 and 8ms in the putamen and between 5 and 7ms in the thalamus. According to the paired t-test results across all participants, the IQR of the CS was significantly lower than the IQR of the Fully in all regions tested. The IQR of the SPICCS was also

significantly lower than the one of CS in all regions except in the thalamus (P=0.065) and the whole gray matter (P=0.047).

The test-retest repeatability experiments showed that the absolute mean T_2 difference between Fully DESS scans could vary from 0.1 to 40 % in the white matter region for all subjects (1 to 15% in the gray matter region). The CS-DESS test-retest returned absolute mean T_2 differences between 0.7 and 11% and between 0.8 and 16% in the white and gray matter regions, respectively. Finally, the SPICCS-DESS scans returned the most repeatable values, with 0.2 to 6% and 0.5 to 5% absolute mean T_2 differences in the white and gray matter regions, respectively. More specifically, the SPICCS-DESS maps had an average of 89% and 81% of voxels that had a T_2 difference below 20% in the white and gray matter regions, respectively, across all volunteers, compared to 78% and 71% for the CS-DESS, and 39% and 37% for the Fully DESS. This gradual improvement is reflected in the representative case in Figure 6a and 6b.
The measurements in the caudate, putamen, thalamus regions also demonstrated a reduction of their mean T_2 test-retest differences for all subjects (Figure 6c) in the CS-DESS and SPICCS-DESS sequences. A summary of these results can be found in Supporting Information Table S1.

In order to characterize the SPICCS-DESS sequence, T_2 estimates of multiple brain regions of the first scan were classified in Table 2. The estimates in the putamen, thalamus and pallidum regions were precise as their T_2 standard deviations were measured between 9 and 13% of their T_2 mean for most subjects. However, the caudate and hippocampus regions presented larger standard deviations (18 to 35% and 17 to 23% margins of error respectively). Looking deeper at their segmentations, voxels with T_2 values over 130ms were detected on the periphery of their segmentations.

The final endeavor was the optimization of the sequence's acquisition time. Omitting 2, and subsequently 4, repetitions, resulted in SPICCS-DESS images that were reconstructed from data acquired in 5min16s and 3min32s, respectively. Both the resulting anatomical and quantitative images were artifact-less and of good quality (Figure 7), albeit slightly compromising on spatial resolution (as seen in the magnified ROIs in Figure 7b and 7c) when compared to 8 repetitions. The T_2 maps were once again homogeneous, and the estimation of T_2 values in the regions of interest remained less variable than the Fully DESS's (Figure 8a) (between 9 and 12ms, between 5 and 8ms, and between 5 and 7ms interquartile ranges in the caudate, putamen and thalamus regions, respectively, for NR=6; between 9 and 14ms, between 5 and 8ms, and between 5 and 8ms interquartile ranges in the caudate, putamen and thalamus regions, respectively, for NR=4, all volunteers included). The increase in IQR with the decreasing number of repetitions was not significant in the putamen region. It was however significant in the caudate and thalamus regions (except between NR=8 and NR=6 in the thalamus with P=0.195). Finally, repeatability was only slightly affected by the reduction of the number of

repetitions (Figure 8b showing the case of a representative volunteer). For all volunteers, the absolute mean T_2 differences were between 0.2 and 4.2% and 0.6 and 6.3% in the white matter and gray matter regions respectively, with NR=6; 0.6 and 8.4% and 1 and 9% absolute mean T_2 differences in the white matter and gray matter regions respectively, with NR=4. NR=6 had an average of 88% and 80% of voxels that had a T_2 difference below 20% in the white and gray matter regions, respectively, across all volunteers, compared to 82% and 76% for the NR=4. These averages were only slightly lower than the ones measured on the original SPICCS-DESS with NR=8 and remained higher than both the Fully DESS's and the CS-DESS's. Absolute mean T_2 differences in the caudate, putamen and thalamus regions also showed slightly lower repeatability with decreasing NR: the average and standard deviation across participants of the mean T2 differences across voxels were 5 ± 4.1%, 7.2 ± 3.8% and 5.8 ± 4.1% for NR=6; and 7.5 ± 5.3%, 8.8 ± 4.7% and 8.3 ± 5.3% for NR=4, for the caudate, putamen and thalamus respectively.

4. DISCUSSION

Proposing a viable and robust 3D DESS T_2 brain mapping sequence is challenging due to its sensitivity to physiological noise which corrupts the acquired data and the resulting estimated maps. This work identified respiration as the main factor in the creation of the ghosting artifacts in the DESS brain images.

The use of retrospective self-gating not only established this correlation but additionally presented a method for artifact correction. Nevertheless, separating the data into seven distinct respiratory phases resulted in the need for repetitions. It is thus the combination of self-gating, CS acceleration and spiral Cartesian reordering that grants this 3D DESS sequence the ability to produce artifact-corrected anatomical and quantitative images whilst maintaining high spatial and temporal resolutions. As a matter of fact, the latter can be further shortened to under 4 minutes without any major drawbacks which could be an interesting feature for non-cooperative patients.

The ghosting artifact observed on the Fully DESS images appeared in the partition encoding direction, with one partition being sampled every 2.4 seconds once all its phase iterations had been completed. This was the first indicator that a slow periodic perturbation such as respiration could be at the root of the image degradation. Combining this information with the respiration-correlated gating signal and the fact that the subjects' heads were firmly set in the coil led to the hypothesis that respiration induced B_0 variation provoked this artifact. Upon further investigation based on numerical simulations, B_0 variations do indeed induce phase and magnitude fluctuations in the $SSFP_{FID}$ and $SSFP_{Echo}$ signals (see Supporting Information Figure S3). The presence of a separate spoiler typically

found in recent DESS works could help mitigate these discrepancies, especially for tissues with high diffusivity such as the cerebral spinal fluid. However, this does not necessarily ensure complete artifact suppression (see Supporting Information Figure S5) and repeatability could thus be compromised as well. Furthermore, introducing additional spoiling gradients results in higher sensitivity to diffusion properties of the tissue and therefore necessitates a correct estimate of the ADC values in the brain for accurate T_2 mapping (see Supporting Information Figures S4 and S5). The current method is therefore preferable in terms of artifact suppression and T_2 estimation. A summary of the impact of B_0 variation and spoiling on DESS signals is detailed in Supporting Information 4.

The processing of the acquired gating signal was performed automatically and efficiently with SSA-FARY, returning noise-less components that best describe the respiratory variation. In fact, it also adds the possibility of including cardiac oscillations into the gating. Indeed, the Fourier transform of the phase of the gating signal displayed a peak around the same frequency as the cardiac frequency (~ 1Hz), albeit less intense than the respiratory peak (see Supporting Information Figure S2). Using SSA-FARY's ability to simultaneously retrieve the respiratory and cardiac oscillations would enable a double gating of the signal. However, a larger amount of data, and therefore a longer acquisition time, would be needed to reach sufficiently filled « double-binned » k-spaces with an adequate spatial resolution.

Even though we believe that B_0 variations are at the root of the image degradation, minor bulk motion induced by respiration or cardiac pulsation should not be excluded as another possible source of artifacts. Nevertheless, this procedure remains valid regardless as it proposes an image reconstruction based on binning according to different stages of a periodic fluctuation, and not an actual correction of the signal. However, the sum of squares of the resulting binned images for SNR maximization would previously necessitate an appropriate co-registration of the images.

The reconstruction of the binned k-spaces' pseudo-random sparse sampling was resolved easily by virtue of the Compressed-Sensing approach, which consequently helped reach the desired acquisition time. The undersampling factor 8 was empirically chosen after having been validated in previous works[30] and compared to factors 6, 10 and 12 on one healthy volunteer (data not shown). The comparison did not yield any notable differences, which was to be expected as the number of repetitions would also change accordingly to maintain the same acquisition time. The optimal regularization parameters were also determined empirically, and might require adjustments according to the different k-space filling rates. Although essential, the Compressed-Sensing approach in this study is not without limitations such as this need for manual adjustment of the reconstruction parameters, the slight blurring introduced into the images and the prerequisite of being able to perform reconstructions externally with Gadgetron.

The golden-step Cartesian sampling with spiral reordering proved quite useful in disrupting the coherence of the respiratory artifact. The ghosting patterns that could originally be seen on the Fully DESS images were « spread out » as noise over the entire volumes. As a result, the act of accumulating repeated k-space lines during the respiratory binning as well as summing the reconstructed images boosted the image quality and the T_2 mapping precision. The benefit of this technique was observed on the anatomical and quantitative images and the improved repeatability measurements, when compared to the CS-DESS. Additional experiments were carried out[35] in order to set the spiral interleaf length equal to the number of phase encoded lines, ensuring a minimal change in gradient intensity to minimize any arising Eddy currents.

The EPG dictionary served as a fitting model that allowed the storage of simulated signals covering a large array of T_1, B_1^+ and T_2 variations. The acquisition of B_1^+ and T_1 maps was necessary for precise T_2 estimations, especially with the DESS sequences being known to be quite sensitive to B_1^+ variation at low flip angles such as the one employed here, a sensitivity which increases with shorter T_1 times[4,8]. Recent works have shown that the DESS sequence can be used for B_0 mapping[10]. Reconstructing one B_0 map and one T_2 map per respiratory phase could potentially improve the accuracy of the T_2 estimates. Indeed, the gold standard Spin-Echo sequence provides longer T_2 values in gray and white matter regions than the current protocol[45–47], which is not the case for phantom experiments (details in Supporting Information Table S1 and Figure S6). This offset could potentially arise from some phenomenon not accounted for in our model, such as magnetization transfer, or variability of respiration amplitude and minor bulk motion that can both disrupt the steady state[48].

As a testament to the SPICCS-DESS's quantitative precision and high spatial resolution, T_2 estimates were assessed on several smaller structures and compared to those found in the Fully and CS-DESS maps. Most regions displayed T_2 standard deviations below 10% of their mean T_2 estimate, as well as lower mean test-retest T_2 differences reflecting a more efficient repeatability between tests than the other two sequences. The high T_2 values found in the caudate and hippocampus regions suggested that part of the cerebral spinal fluid had been included in their respective segmentations, which in turn led to higher standard deviations. The hippocampus is also known to possess several internal substructures[49,50], which could further explain its T_2 inhomogeneity.

An extremely important aspect of the current study is the reliable and improved intra-subject repeatability when compared to the Fully DESS. A subsequent step to this study would be to extend the patient age range in order to get the full scope of the sequence's T_2 quantification ability and to apply it for the diagnosis and monitoring of pathologies such as multiple sclerosis.

Reducing the number of repetitions while maintaining efficient repeatability proved to be a promising aspect of the method as it both shortens acquisition time and leads to a smaller chance of patient movement during the scan. Investigating higher acceleration factors could be particularly interesting as there would be more options to choose from in terms of number of repetitions. For instance, with an undersampling factor of 12, one could set the number of repetitions to 12, 11, 10, 9…etc. A detailed study of this aspect of the sequence would therefore be very useful depending on the compromise one wishes to make between spatial and temporal resolutions.

The ability to shorten the acquisition time thus shows great promise, especially when considering submillimetric spatial resolutions. This leads to the idea of transferring the sequence to a higher magnetic field strength scanner (7T), especially since the low flip angles used here decrease the likelihood of specific absorption rate issues.

Availability of the DESS sequence and reconstruction on a clinical scanner is not currently possible in clinical routine. That is why the sequence and the reconstruction codes developed in this study can be provided upon request.

5. CONCLUSIONS

By blending different cartesian encoding and reconstruction schemes into a T_2 quantification protocol, a 3D DESS sequence has been optimized with respect to its sensitivity to B_0 variation and its T_2 mapping repeatability. The gradual implementation of retrospective self-gating, golden-step spiral reordering and Compressed-Sensing acceleration allowed an in-depth analysis of the respiratory artifact correction. A clear improvement was consequently observed in the image and map quality, as well as the voxel-wise T_2 distribution and repeatability. The SPICCS-DESS sequence therefore allows a rapid and robust estimation of the T_2 parameter in the whole brain, facilitating the longitudinal monitoring of cerebral pathologies and treatments.

ACKNOWLEDGEMENTS

This work was supported by the French National Research Agency (ANR-19-CE19-0014).

REFERENCES

1. Bruder H, Fischer H, Graumann R, Deimling M. A new steady-state imaging sequence for simultaneous acquisition of two MR images with clearly different contrasts. *Magn Reson Med*. 1988;7(1):35-42. doi:https://doi.org/10.1002/mrm.1910070105

2. Lee SY, Cho ZH. Fast SSFP gradient echo sequence for simultaneous acquisitions of FID and echo signals. *Magn Reson Med*. 1988;8(2):142-150. doi:https://doi.org/10.1002/mrm.1910080204
3. Redpath TW, Jones RA. FADE–A new fast imaging sequence. *Magn Reson Med*. 1988;6(2):224-234. doi:https://doi.org/10.1002/mrm.1910060211
4. Chaudhari AS, Black MS, Eijgenraam S, et al. Five-minute knee MRI for simultaneous morphometry and T2 relaxometry of cartilage and meniscus and for semiquantitative radiological assessment using double-echo in steady-state at 3T. *J Magn Reson Imaging*. 2018;47(5):1328-1341. doi:https://doi.org/10.1002/jmri.25883
5. Chaudhari AS, Sveinsson B, Moran CJ, et al. Imaging and T2 relaxometry of short-T2 connective tissues in the knee using ultrashort echo-time double-echo steady-state (UTEDESS). *Magn Reson Med*. 2017;78(6):2136-2148. doi:https://doi.org/10.1002/mrm.26577
6. Jordan CD, McWalter EJ, Monu UD, et al. Variability of CubeQuant T1ρ, quantitative DESS T2, and cones sodium MRI in knee cartilage. *Osteoarthritis Cartilage*. 2014;22(10):1559-1567. doi:10.1016/j.joca.2014.06.001
7. Peterfy CG, Schneider E, Nevitt M. The osteoarthritis initiative: report on the design rationale for the magnetic resonance imaging protocol for the knee. *Osteoarthritis Cartilage*. 2008;16(12):1433-1441. doi:10.1016/j.joca.2008.06.016
8. Welsch GH, Scheffler K, Mamisch TC, et al. Rapid estimation of cartilage T2 based on double echo at steady state (DESS) with 3 Tesla. *Magn Reson Med*. 2009;62(2):544-549. doi:https://doi.org/10.1002/mrm.22036
9. Staroswiecki E, Granlund KL, Alley MT, Gold GE, Hargreaves BA. Simultaneous estimation of T2 and apparent diffusion coefficient in human articular cartilage in vivo with a modified three-dimensional double echo steady state (DESS) sequence at 3 T. *Magn Reson Med*. 2012;67(4):1086-1096. doi:https://doi.org/10.1002/mrm.23090
10. Barbieri M, Chaudhari AS, Moran CJ, Gold GE, Hargreaves BA, Kogan F. A method for measuring B0 field inhomogeneity using quantitative double-echo in steady-state. *Magn Reson Med*. 2023;89(2):577-593. doi:10.1002/mrm.29465
11. Nataraj G, Nielsen JF, Gao M, Fessler JA. Fast, Precise Myelin Water Quantification using DESS MRI and Kernel Learning. September 2018. doi:10.48550/arXiv.1809.08908
12. Sveinsson B, Chaudhari AS, Gold GE, Hargreaves BA. A simple analytic method for estimating T2 in the knee from DESS. *Magn Reson Imaging*. 2017;38:63-70. doi:10.1016/j.mri.2016.12.018
13. Moran CJ, Cheng JY, Sandino CM, et al. Diffusion-weighted double-echo steady-state with a three-dimensional cones trajectory for non-contrast-enhanced breast MRI. *J Magn Reson Imaging*. 2021;53(5):1594-1605. doi:10.1002/jmri.27492
14. Dregely I, Margolis DAJ, Sung K, et al. Rapid quantitative T2 mapping of the prostate using three-dimensional dual echo steady state MRI at 3T. *Magn Reson Med*. 2016;76(6):1720-1729. doi:https://doi.org/10.1002/mrm.26053
15. Gras V, Farrher E, Grinberg F, Shah NJ. Diffusion-weighted DESS protocol optimization for simultaneous mapping of the mean diffusivity, proton density and relaxation times at 3 Tesla. *Magn Reson Med*. 2017;78(1):130-141. doi:https://doi.org/10.1002/mrm.26353
16. Wu PH, Cheng CC, Wu ML, Chao TC, Chung HW, Huang TY. Effects of RF profile on precision of quantitative T2 mapping using dual-echo steady-state acquisition. *Magn Reson Imaging*. 2014;32(1):102-106. doi:10.1016/j.mri.2013.10.002
17. Nataraj G, Nielsen JF, Fessler JA. Model-based estimation of T2 maps with dual-echo steady-state MR imaging. In: *2014 IEEE International Conference on Image Processing (ICIP)*. Paris: IEEE; 2014:1877-1881. doi:10.1109/ICIP.2014.7025376
18. Knight MJ, McCann B, Tsivos D, Dillon S, Coulthard E, Kauppinen RA. Quantitative T2 mapping of white matter: applications for ageing and cognitive decline. *Phys Med Biol*. 2016;61(15):5587-5605. doi:10.1088/0031-9155/61/15/5587
19. Rugg-Gunn FJ, Boulby PA, Symms MR, Barker GJ, Duncan JS. Whole-brain T2 mapping demonstrates occult abnormalities in focal epilepsy. *Neurology*. 2005;64(2):318-325. doi:10.1212/01.WNL.0000149642.93493.F4
20. Jacobs MA, Mitsias P, Soltanian-Zadeh H, et al. Multiparametric MRI Tissue Characterization in Clinical Stroke With Correlation to Clinical Outcome. *Stroke*. 2001;32(4):950-957.

doi:10.1161/01.STR.32.4.950
21. Armspach JP, Gounot D, Rumbach L, Chambron J. In vivo determination of multiexponential T2 relaxation in the brain of patients with multiple sclerosis. *Magn Reson Imaging*. 1991;9(1):107-113. doi:10.1016/0730-725X(91)90104-T
22. Stevenson VL, Parker GJM, Barker GJ, et al. Variations in T1 and T2 relaxation times of normal appearing white matter and lesions in multiple sclerosis. *J Neurol Sci*. 2000;178(2):81-87. doi:10.1016/S0022-510X(00)00339-7
23. Woermann F, Barker G, Birnie K, Meencke H, Duncan J. Regional changes in hippocampal T2 relaxation and volume: a quantitative magnetic resonance imaging study of hippocampal sclerosis. *J Neurol Neurosurg Psychiatry*. 1998;65(5):656-664.
24. Moran CJ, Granlund KL, Sveinsson B, Alley MT, Daniel BL, Hargreaves BA. Respiration Induced B0 Variation in Double Echo Steady State Imaging (DESS) in the Breast. *Proc Intl Soc Mag Reson Med 23*. 2015:498.
25. Ehman R, McNamara M, Pallack M, Hricak H, Higgins C. Magnetic resonance imaging with respiratory gating: techniques and advantages. *Am J Roentgenol*. 1984;143(6):1175-1182. doi:10.2214/ajr.143.6.1175
26. Liu Y, Yin FF, Czito BG, Bashir MR, Cai J. T2-weighted four dimensional magnetic resonance imaging with result-driven phase sorting. *Med Phys*. 2015;42(8):4460-4471. doi:10.1118/1.4923168
27. Crowe ME, Larson AC, Zhang Q, et al. Automated rectilinear self-gated cardiac cine imaging. *Magn Reson Med*. 2004;52(4):782-788. doi:10.1002/mrm.20212
28. Han F, Zhou Z, Cao M, Yang Y, Sheng K, Hu P. Respiratory motion-resolved, self-gated 4D-MRI using rotating cartesian k-space (ROCK). *Med Phys*. 2017;44(4):1359-1368. doi:10.1002/mp.12139
29. Larson AC, White RD, Laub G, McVeigh ER, Li D, Simonetti OP. Self-gated cardiac cine MRI. *Magn Reson Med*. 2004;51(1):93-102. doi:10.1002/mrm.10664
30. Trotier AJ, Dilharreguy B, Anandra S, et al. The Compressed Sensing MP2RAGE as a Surrogate to the MPRAGE for Neuroimaging at 3 T. *Invest Radiol*. 2022;57(6):366-378. doi:10.1097/RLI.0000000000000849
31. Mussard E, Hilbert T, Forman C, Meuli R, Thiran JP, Kober T. Accelerated MP2RAGE imaging using Cartesian phyllotaxis readout and compressed sensing reconstruction. *Magn Reson Med*. 2020;84(4):1881-1894. doi:10.1002/mrm.28244
32. Godino-Moya A, Royuela-del-Val J, Usman M, et al. Space-time variant weighted regularization in compressed sensing cardiac cine MRI. *Magn Reson Imaging*. 2019;58:44-55. doi:10.1016/j.mri.2019.01.005
33. Varela-Mattatall G, Baron CA, Menon RS. Automatic determination of the regularization weighting for wavelet-based compressed sensing MRI reconstructions. *Magn Reson Med*. 2021;86(3):1403-1419. doi:10.1002/mrm.28812
34. Prieto C, Doneva M, Usman M, et al. Highly efficient respiratory motion compensated free-breathing coronary mra using golden-step Cartesian acquisition. *J Magn Reson Imaging*. 2015;41(3):738-746. doi:10.1002/jmri.24602
35. Kadalie E, Trotier AJ, Corbin N, Miraux S, Ribot EJ. Increasing the repeatability of DESS 3D brain T2 mapping with optimized k-space sampling order. *Proc. Intl. Soc. Mag. Reson. Med. 31*. 2023:5091.
36. Hansen MS, Sørensen TS. Gadgetron: An open source framework for medical image reconstruction. *Magn Reson Med*. 2013;69(6):1768-1776. doi:10.1002/mrm.24389
37. Uecker M, Rosenzweig S, Holme HCM, et al. mrirecon/bart: version 0.6.00. July 2020. doi:10.5281/zenodo.3934312
38. Rosenzweig S, Scholand N, Holme HCM, Uecker M. Cardiac and Respiratory Self-Gating in Radial MRI using an Adapted Singular Spectrum Analysis (SSA-FARY). *IEEE Trans Med Imaging*. 2020;39(10):3029-3041. doi:10.1109/TMI.2020.2985994
39. Weigel M. Extended phase graphs: Dephasing, RF pulses, and echoes - pure and simple. *J Magn Reson Imaging*. 2015;41(2):266-295. doi:https://doi.org/10.1002/jmri.24619
40. Hennig J. Echoes—how to generate, recognize, use or avoid them in MR-imaging sequences. Part I: Fundamental and not so fundamental properties of spin echoes. *Concepts Magn Reson*.

1991;3(3):125-143. doi:https://doi.org/10.1002/cmr.1820030302
41. Hennig J. Echoes—how to generate, recognize, use or avoid them in MR-imaging sequences. Part II: Echoes in imaging sequences. *Concepts Magn Reson*. 1991;3(4):179-192. doi:https://doi.org/10.1002/cmr.1820030402
42. Lamy J, de Sousa PL. Sycomore: an MRI simulation toolkit. *Proc Intl Soc Mag Reson Med 28*. 2020:1038.
43. Ashburner J, Friston KJ. Unified segmentation. *NeuroImage*. 2005;26(3):839-851. doi:10.1016/j.neuroimage.2005.02.018
44. Manjón JV, Coupé P. volBrain: An Online MRI Brain Volumetry System. *Front Neuroinformatics*. 2016;10:30. doi:10.3389/fninf.2016.00030
45. Ben-Eliezer N, Sodickson DK, Block KT. Rapid and accurate T2 mapping from multi–spin-echo data using Bloch-simulation-based reconstruction. *Magn Reson Med*. 2015;73(2):809-817. doi:10.1002/mrm.25156
46. Nöth U, Shrestha M, Schüre JR, Deichmann R. Quantitative in vivo T2 mapping using fast spin echo techniques – A linear correction procedure. *NeuroImage*. 2017;157:476-485. doi:10.1016/j.neuroimage.2017.06.017
47. Snyder J, McPhee KC, Wilman AH. T2 quantification in brain using 3D fast spin-echo imaging with long echo trains. *Magn Reson Med*. 2022;87(5):2145-2160. doi:10.1002/mrm.29113
48. O'Halloran R, Aksoy M, Aboussouan E, Peterson E, Van A, Bammer R. Real-time correction of rigid body motion-induced phase errors for diffusion-weighted steady-state free precession imaging. *Magn Reson Med*. 2015;73(2):565-576. doi:https://doi.org/10.1002/mrm.25159
49. DeKraker J, Ferko KM, Lau JC, Köhler S, Khan AR. Unfolding the hippocampus: An intrinsic coordinate system for subfield segmentations and quantitative mapping. *NeuroImage*. 2018;167:408-418. doi:10.1016/j.neuroimage.2017.11.054
50. Winterburn JL, Pruessner JC, Chavez S, et al. A novel in vivo atlas of human hippocampal subfields using high-resolution 3T magnetic resonance imaging. *NeuroImage*. 2013;74:254-265. doi:10.1016/j.neuroimage.2013.02.003

TABLES

	Filling rate											
Nb of bins	**Single bin**		**5 bins**		**6 bins**		**7 bins**		**8 bins**		**9 bins**	
Object	**Fully**	**CS8 NR1**	**CS-DESS**	**SPICCS-DESS**	**CS-DESS**	**SPICCS-DESS**	**CS-DESS**	**SPICCS-DESS**	**CS-DESS**	**SPICCS-DESS**	**CS-DESS**	**SPICCS-DESS**
k-space	100 %	13,4 %	17.6±0.7%	17.7±0.2%	15.0±0.6%	15.2±0.2%	13.2±0.5%	13.3±0.1%	11.7±0.4%	11.8±0.1%	10.5±0.4%	10.6±0.1%
k-space center	100 %	100 %	82.4±4.8%	82.6±4.0%	75.9±3.7%	76.2±4.4%	70.4±3.4%	70.2±3.7%	65.2±3.0%	65.0±3.7%	60.6±2.8%	60.2±3.4%

Table 1: Average filling rates of the SPICCS-DESS k-spaces and k-space centers with different numbers of bins across all volunteers.

		T_2 measurements (ms)						
Subject	**Test/Retest**	**White Matter**	**Gray Matter**	**Caudate**	**Putamen**	**Thalamus**	**Pallidum**	**Hippocampus**
1	Test	47.5 ± 5.3 ms	61.6 ± 11.1 ms	52.9 ± 14.6 ms	42.1 ± 5.0 ms	42.5 ± 4.6 ms	30.5 ± 3.2 ms	67.3 ± 14.4 ms
	Retest	49.0 ± 6.0 ms	62.0 ± 10.7 ms	58.1 ± 17.2 ms	40.9 ± 5.3 ms	46.3 ± 5.7 ms	30.4 ± 4.0 ms	66.0 ± 13.6 ms
2	Test	42.3 ± 6.7 ms	53.3 ± 10.4 ms	44.9 ± 12.8 ms	39.1 ± 4.0 ms	36.1 ± 4.1 ms	25.4 ± 2.9 ms	56.5 ± 10.8 ms
	Retest	42.0 ± 5.7 ms	54.8 ± 9.3 ms	47.4 ± 16.5 ms	38.4 ± 4.2 ms	40.7 ± 4.9 ms	26.6 ± 3.5 ms	59.4 ± 11.3 ms
3	Test	40.5 ± 5.3 ms	55.1 ± 9.6 ms	47.7 ± 14.1 ms	36.0 ± 4.1 ms	40.0 ± 4.5 ms	27.9 ± 2.9 ms	58.5 ± 13.1 ms
	Retest	42.0 ± 5.6 ms	57.2 ± 10.2 ms	51.7 ± 16.6 ms	38.6 ± 4.4 ms	43.3 ± 5.0 ms	29.4 ± 2.9 ms	63.1 ± 13.9 ms
4	Test	49.4 ± 7.2 ms	66.2 ± 11.1 ms	58.9 ± 13.7 ms	51.0 ± 5.0 ms	48.6 ± 5.1 ms	35.5 ± 4.3 ms	69.4 ± 13.1 ms
	Retest	47.2 ± 6.2 ms	62.9 ± 10.2 ms	57.1 ± 13.1 ms	45.3 ± 4.9 ms	48.6 ± 5.8 ms	31.9 ± 3.8 ms	61.4 ± 10.8 ms
5	Test	44.3 ± 6.0 ms	56.1 ± 9.8 ms	53.7 ± 9.8 ms	49.7 ± 5.9 ms	44.4 ± 4.7 ms	34.3 ± 4.4 ms	62.0 ± 12.4 ms
	Retest	43.7 ± 5.5 ms	55.7 ± 9.4 ms	50.8 ± 10.6 ms	46.1 ± 4.9 ms	45.4 ± 4.5 ms	29.6 ± 4.3 ms	59.5 ± 10.3 ms
6	Test	44.0 ± 5.3 ms	58.9 ± 10.1 ms	49.7 ± 15.7 ms	42.7 ± 4.6 ms	47.4 ± 7.2 ms	29.6 ± 3.9 ms	60.4 ± 12.2 ms
	Retest	45.7 ± 5.1 ms	59.4 ± 9.6 ms	55.7 ± 17.2 ms	44.9 ± 5.2 ms	46.3 ± 6.1 ms	31.8 ± 4.1 ms	66.0 ± 14.2 ms
7	Test	46.7 ± 5.1 ms	61.1 ± 9.9 ms	51.8 ± 10.1 ms	45.8 ± 4.5 ms	44.6 ± 5.2 ms	31.2 ± 3.4 ms	66.6 ± 11.6 ms
	Retest	43.9 ± 4.9 ms	57.9 ± 9.7 ms	47.6 ± 9.9 ms	43.2 ± 4.1 ms	43.4 ± 4.5 ms	29.5 ± 3.3 ms	61.6 ± 11.7 ms
8	Test	45.1 ± 6.1 ms	63.3 ± 14.1 ms	46.9 ± 12.4 ms	40.6 ± 5.1 ms	41.5 ± 4.8 ms	30.1 ± 3.9 ms	67.9 ± 15.7 ms
	Retest	42.7 ± 6.2 ms	59.9 ± 12.7 ms	44.8 ± 10.9 ms	35.9 ± 4.9 ms	40.6 ± 5.3 ms	27.5 ± 3.1 ms	61.1 ± 13.0 ms

Table 2: SPICCS-DESS T_2 test-retest values (mean ± standard deviation) measured in the various segmented brain structures, for each volunteer.

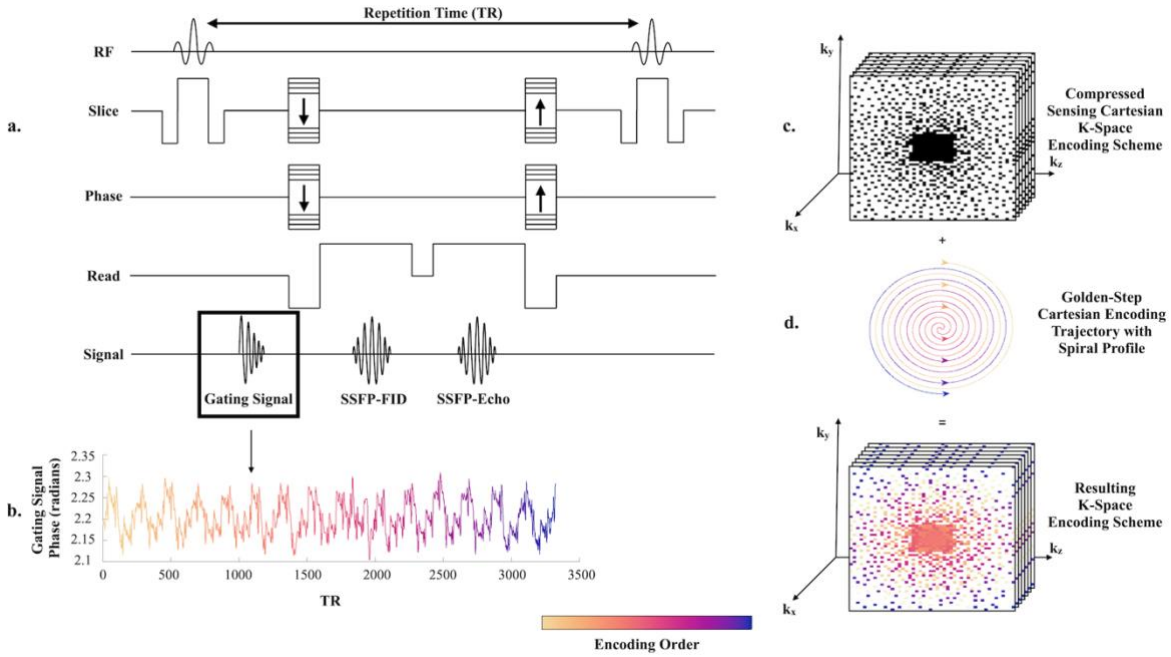

Figure 1: a. DESS chronogram and acquisition specifics, with the insertion of the gating module (Gated DESS). b. The gating signal (4 points in the center of the k-space) was acquired in the same TR as the $SSFP_{FID}$ and $SSFP_{Echo}$ echoes, and the phase of this signal was analyzed. c. A Compressed-Sensing mask was applied to obtain undersampled images. At this step, the sequence is called CS-DESS. d. A further modification of the encoding was added through a Golden-Step Cartesian Encoding trajectory with spiral profiling. The resulting k-space encoding scheme is presented, at which point the sequence is now called SPICCS-DESS.

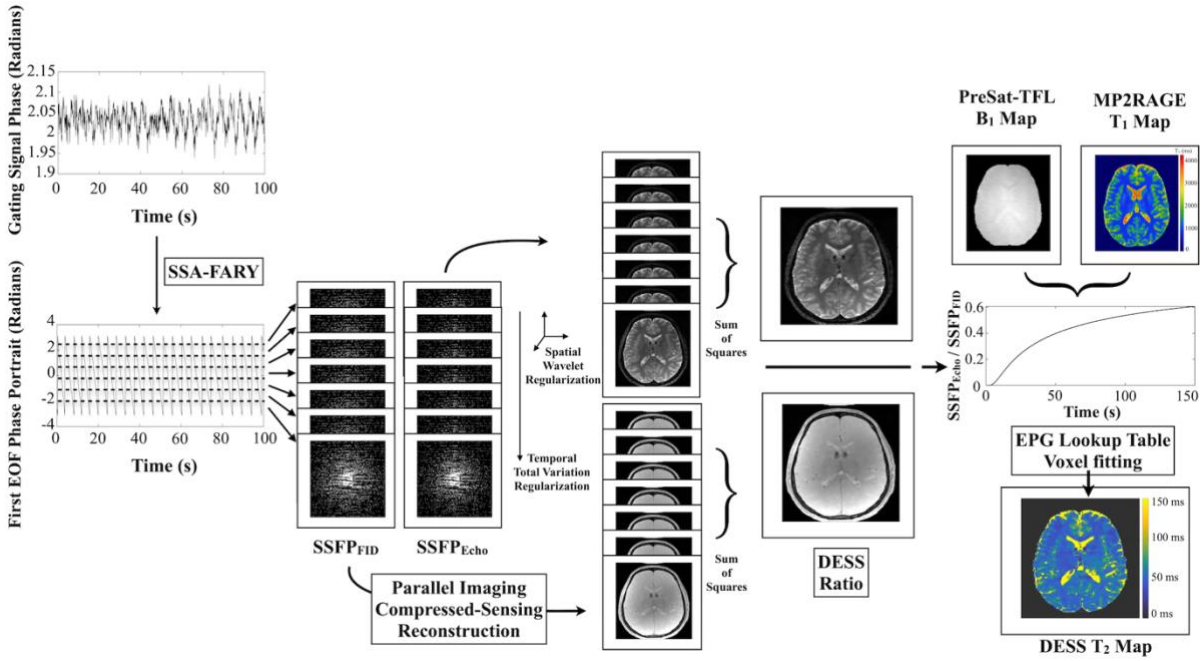

Figure 2: Full reconstruction pipeline for the CS-DESS and SPICCS-DESS sequences. The gating signal was processed with SSA-FARY and divided into 7 bins here in order to assemble new k-spaces. The k-spaces were undersampled, requiring Compressed-Sensing parallel imaging reconstruction with spatial and temporal regularizations (contrary to the fully sampled k-spaces of the Gated DESS). $SSFP_{FID}$ and $SSFP_{Echo}$ images were reconstructed and summed up respectively. The ratio of the two resulting images were then fitted voxel-wise to a Lookup Table simulated with the EPG framework (and optimized with the B_1 and T_1 maps acquired during the exam) in order to produce the T_2 map.

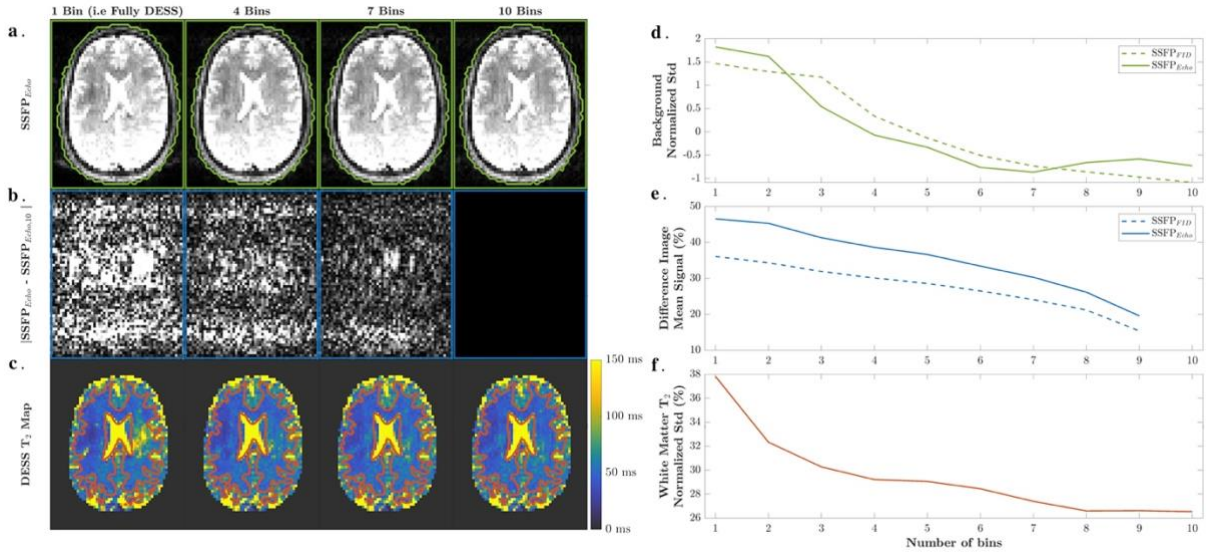

Figure 3: a. The 3mm Gated DESS data reconstructed with 1 to 10 respiratory bins. Image contrast was adjusted in order to properly observe the ghosting artifact. The green ROI contours the entire background of the Gated DESS $SSFP_{Echo}$ images. d. Evolution of the normalized standard deviation in this ROI with respect to the number of bins, for both the $SSFP_{FID}$ and $SSFP_{Echo}$ images. b. Absolute difference images of the Gated DESS $SSFP_{Echo}$ images minus the reference image (here the 10 bins Gated DESS). The blue squared ROI was used to highlight the fact that the whole 3D dataset was analyzed. e. Evolution of the mean signal in this ROI with respect to the number of bins. c. The corresponding Gated DESS T_2 maps, with the white matter region highlighted in red. f. Evolution of this region's T_2 normalized standard deviation in the Gated DESS T_2 maps with respect to the number of bins.

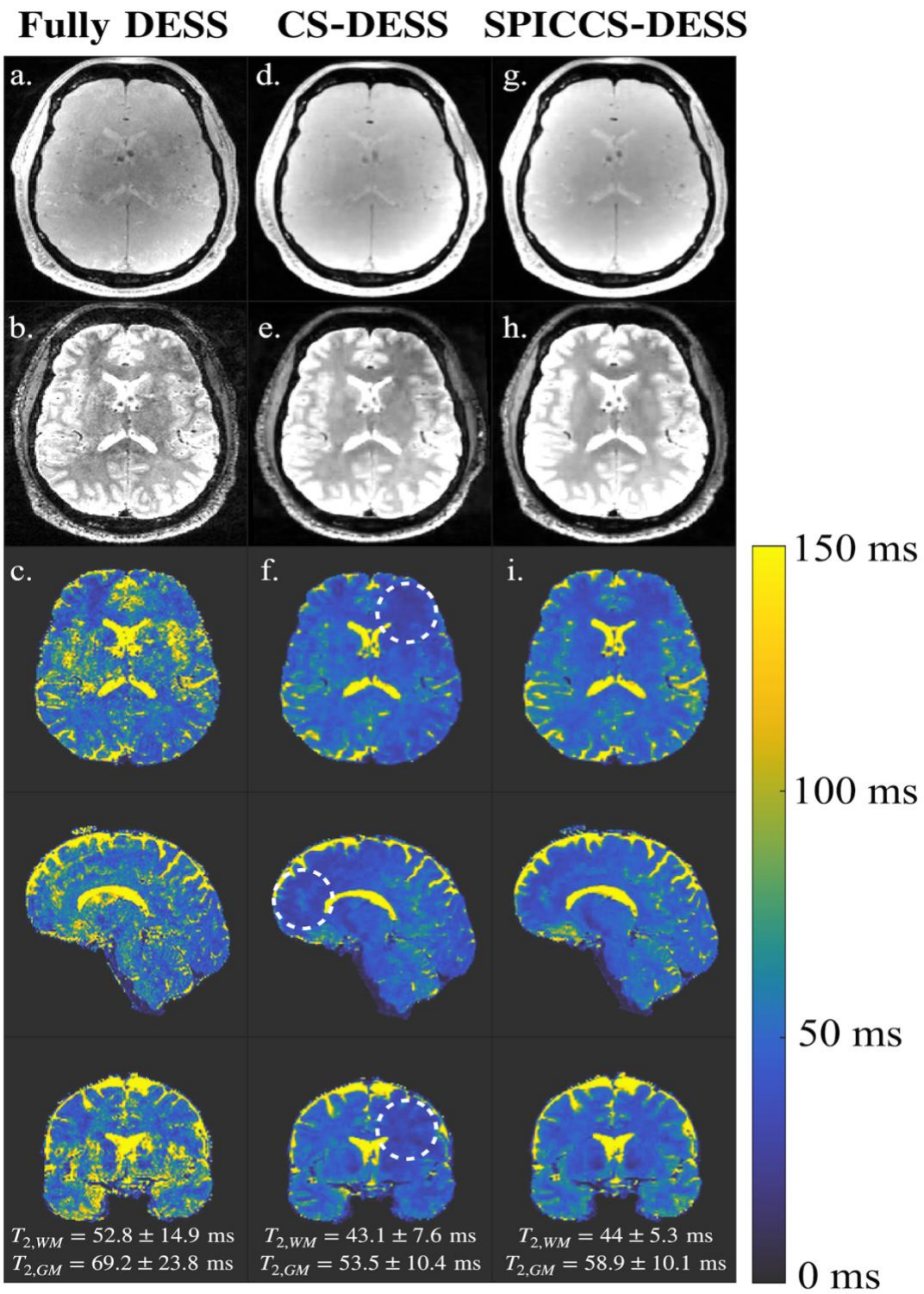

Figure 4: Comparison between Fully DESS (a-c), CS-DESS (d-f), and SPICCS-DESS (g-i) images in all spatial directions for a representative subject. The highlighted region on the CS-DESS T_2 map shows the area of the right hemisphere with lower T_2 values due to incomplete artifact suppression. a., d., g.: $SSFP_{FID}$ images. b., e., h.: $SSFP_{Echo}$ images. Image contrast was adjusted in order to properly observe the ghosting artifact. c., f., i.: Resulting T_2 maps.

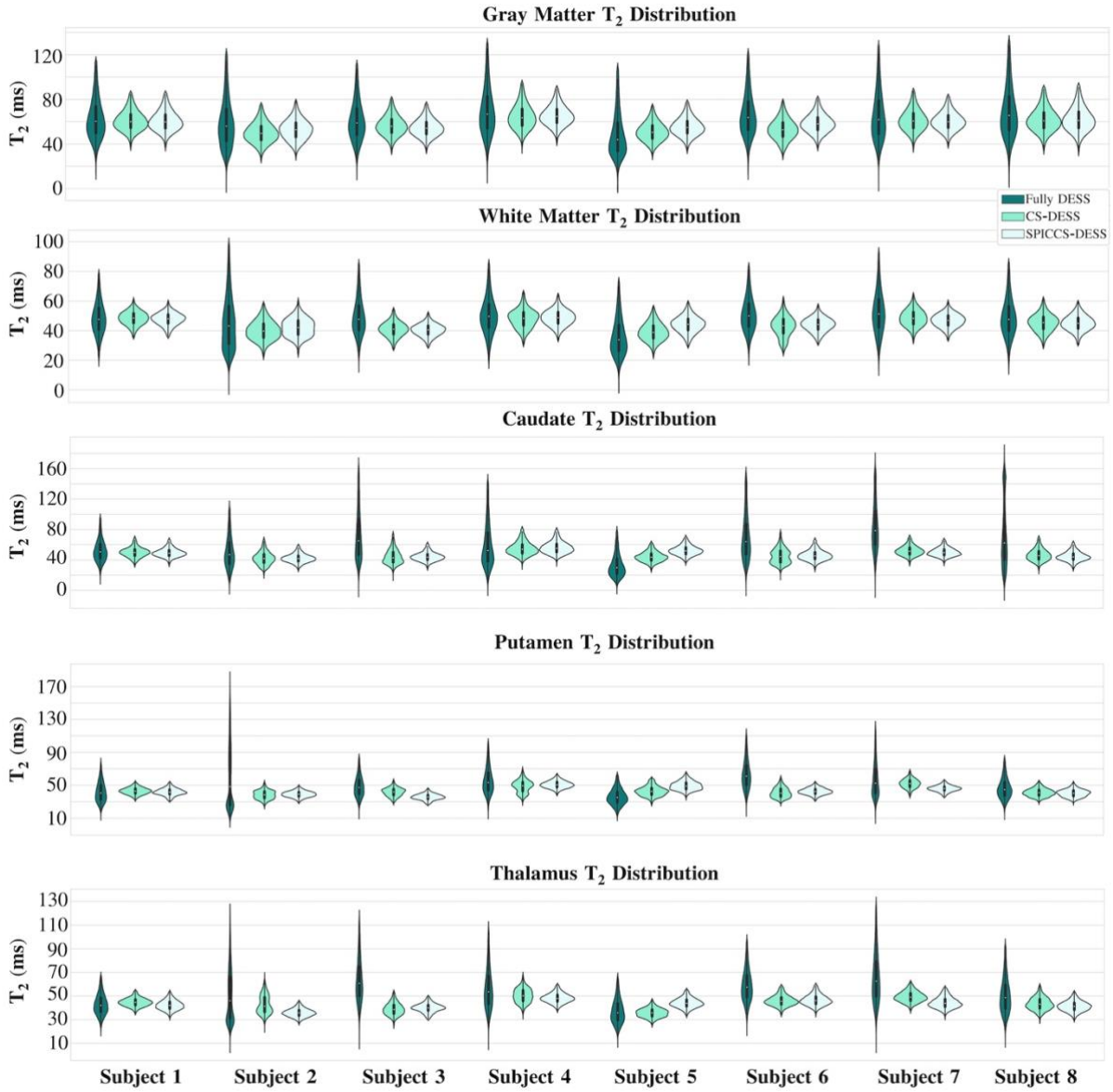

Figure 5: Violin plots for each subject regrouping all voxels in the gray matter, white matter, caudate, putamen and thalamus regions for the Fully (dark cyan), CS (cyan) and SPICCS-DESS (light cyan) sequences.

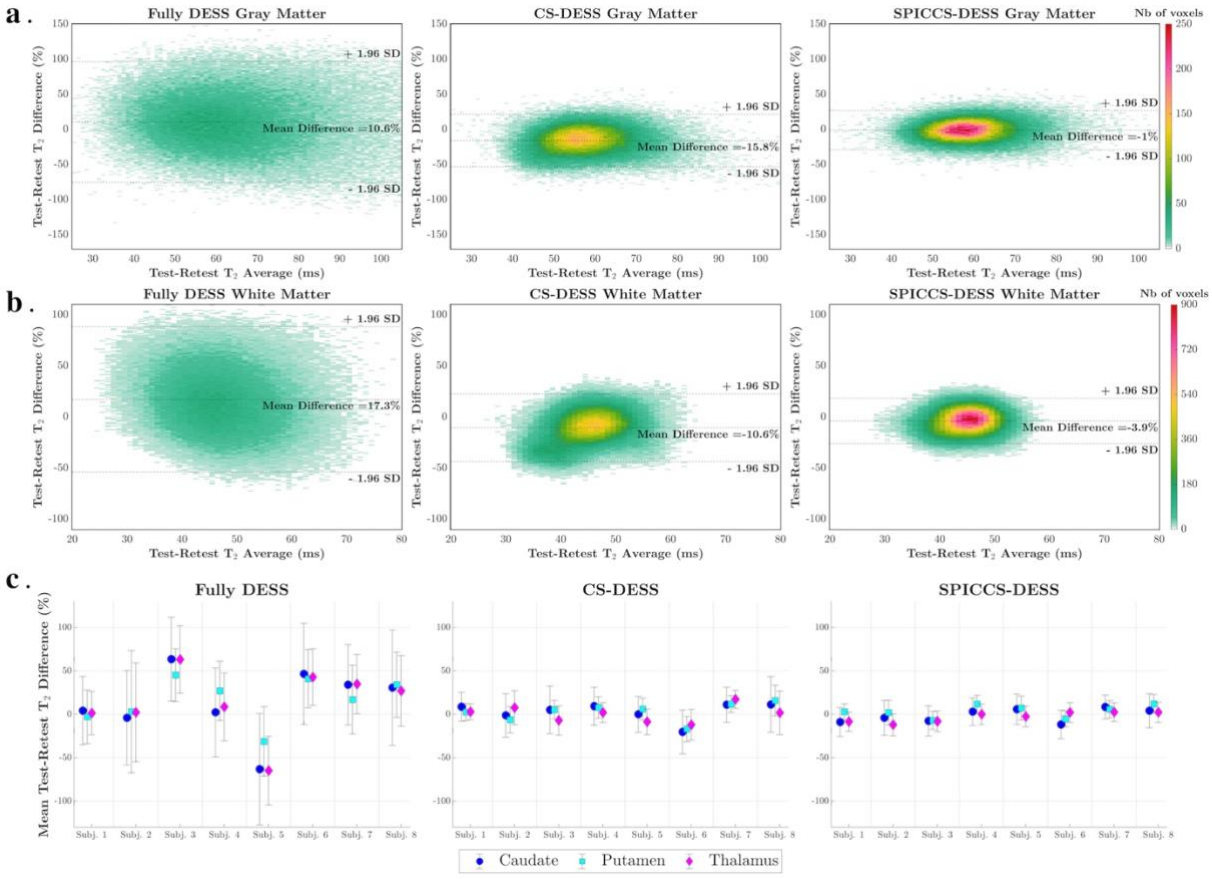

Figure 6: Bland-Altman plots in a. gray and b. white matter areas depicting test-retest T_2 normalized differences with respect to the T_2 averages, from the Fully DESS (left), the CS-DESS (middle) and the SPICCS-DESS (right), for the representative subject (Subject 6). c. *M*, the mean test-retest T_2 normalized differences of the three segmented substructures for all subjects, from the Fully DESS (left), the CS-DESS (middle) and the SPICCS-DESS (right).

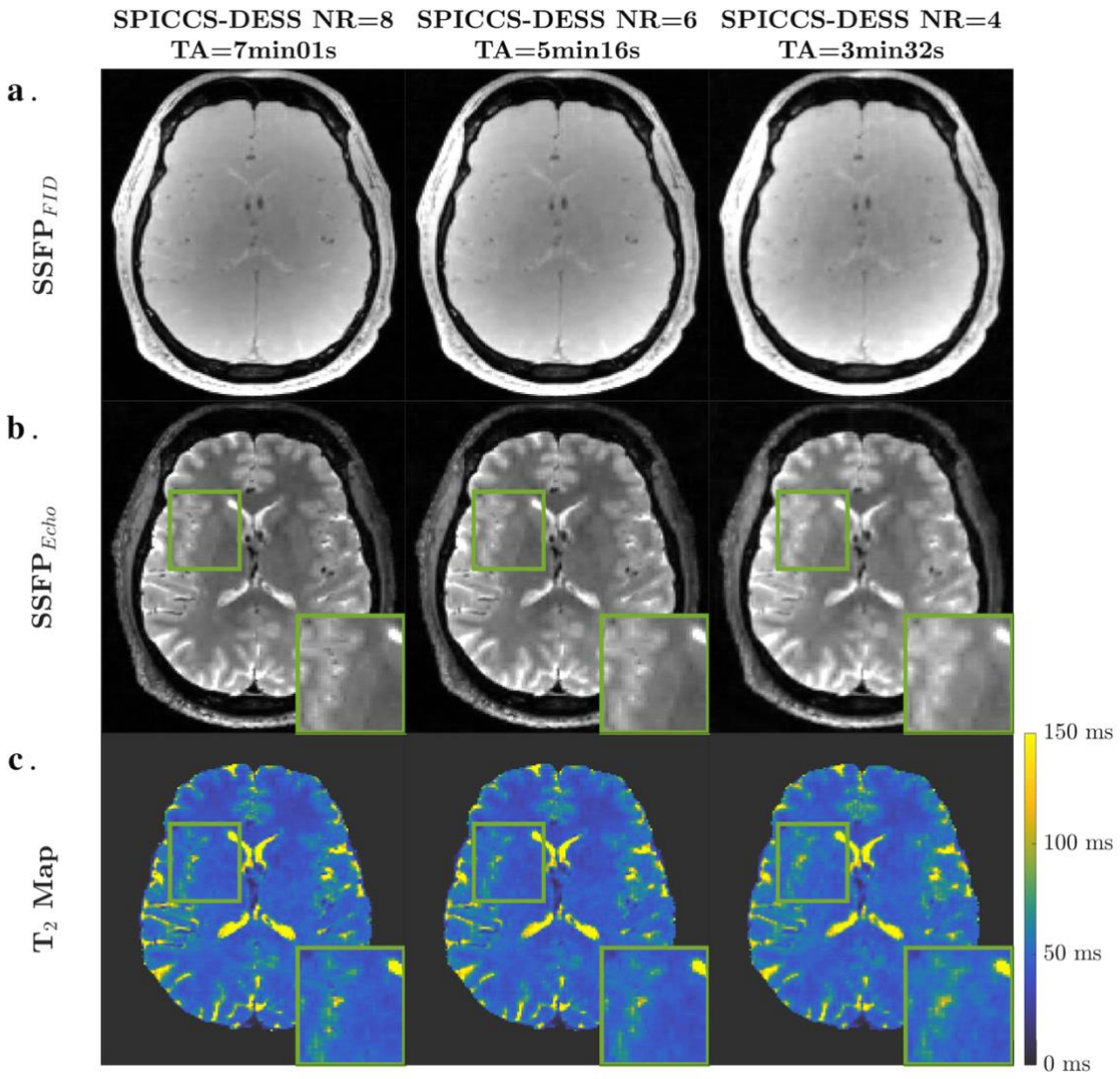

Figure 7: Comparison of the SPICCS-DESS with NR=8, 6, 4. a. $SSFP_{FID}$ images. b. $SSFP_{Echo}$ images. c. Corresponding T_2 maps. The green ROI in the $SSFP_{Echo}$ and T_2 maps was magnified in order to show the slight decrease in image sharpness resulting from less repetitions being used.

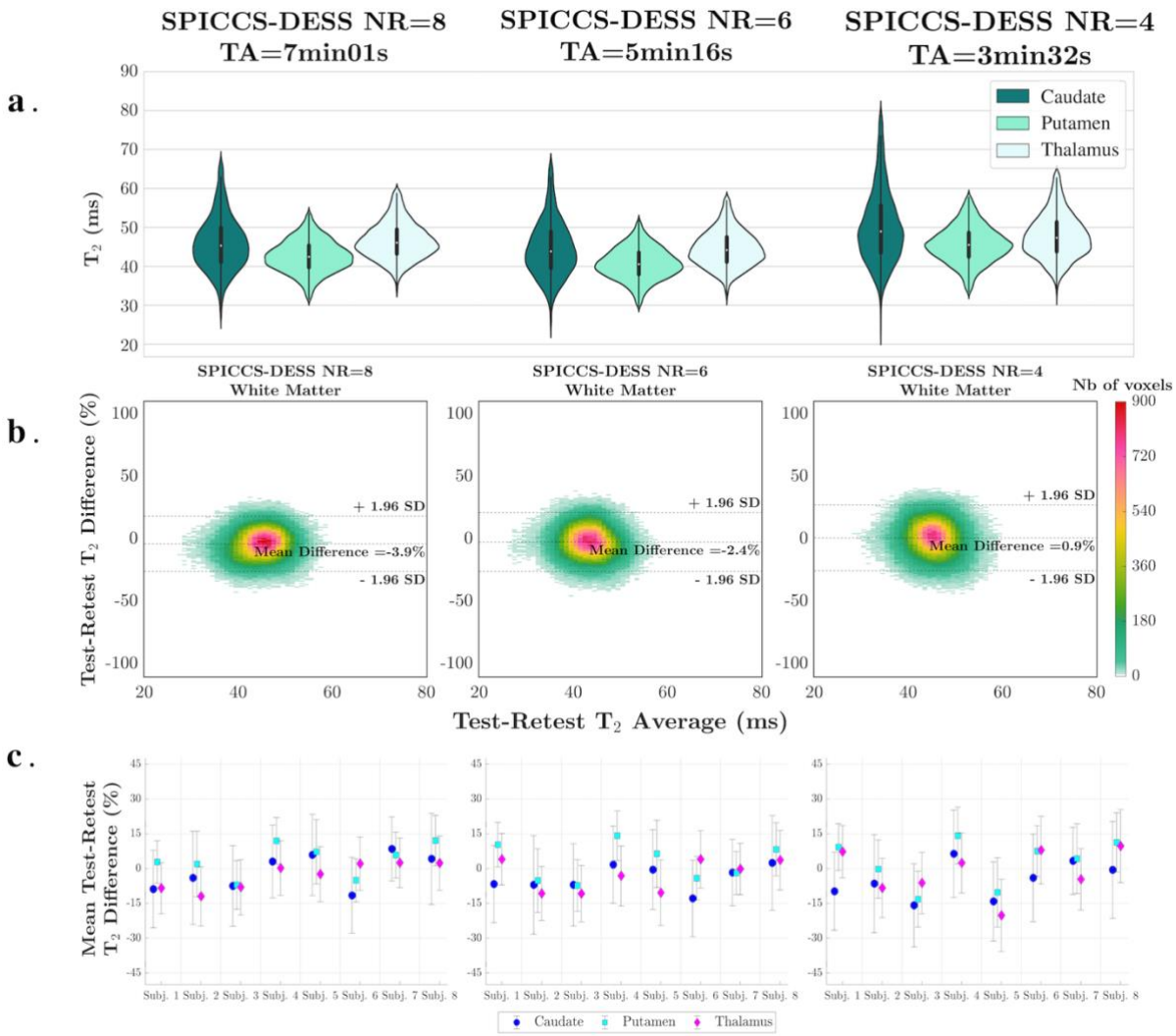

Figure 8: Comparison of the SPICCS-DESS with NR=8, 6, 4. a. Violin plots depicting the T_2 distribution in the caudate, putamen and thalamus regions. b. Bland-Altman plots in the white matter area depicting test-retest T_2 difference with respect to the T_2 average. c. Mean test-retest T_2 differences (*M*) of the three segmented substructures for all subjects.

Supporting Information 1: Fully DESS artifact

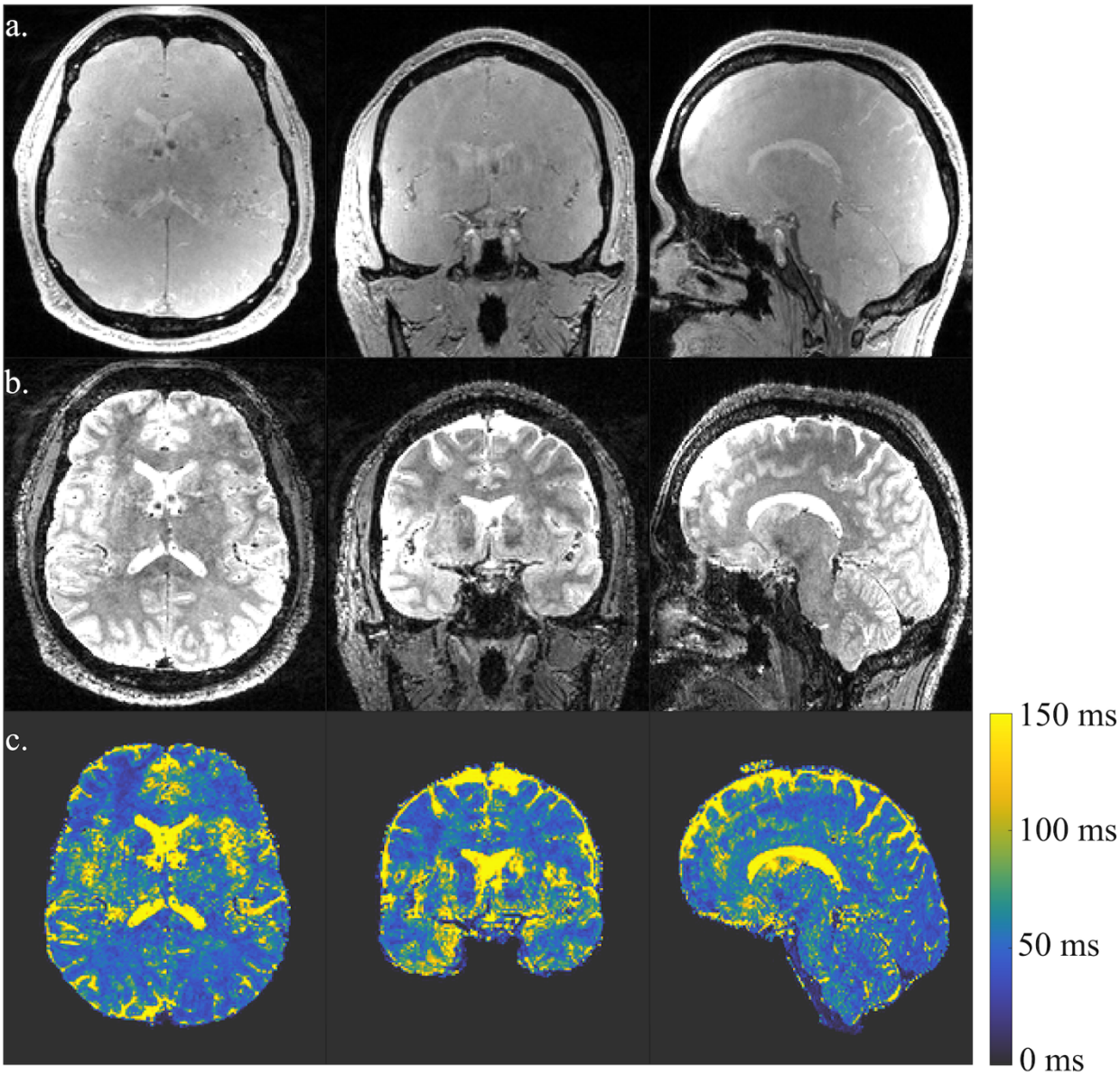

Figure S1: Fully DESS images in all spatial directions for a representative subject. a. $SSFP_{FID}$ images. b. $SSFP_{Echo}$ images. c. Resulting T_2 maps. A ghosting artifact can be observed on all images, notably corrupting the $SSFP_{Echo}$ images and the T_2 maps.

Supporting Information 2: Respiration vs Self-Gating signal

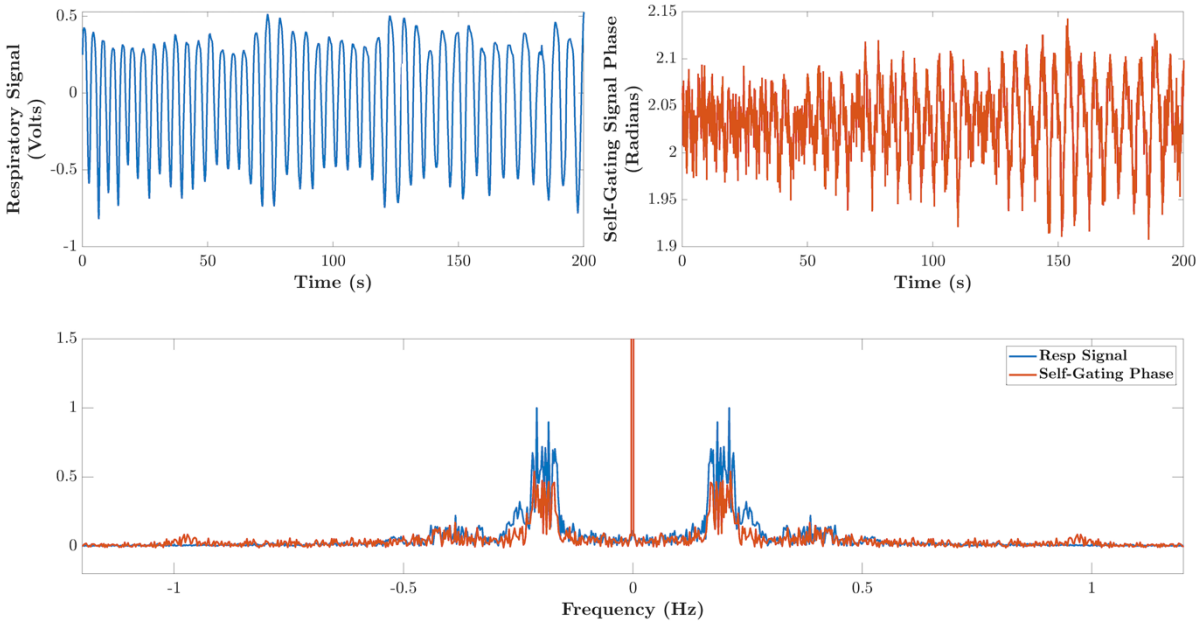

Figure S2*:* a. Respiratory traces obtained with the respiratory belt. b. Phase of the simultaneously acquired gating signal. c. The corresponding spectra of both signals further emphasized the correlation with peaks appearing around 0.17-0.22 Hz.

Supporting Information 3: Mean test-retest T_2 differences

Region	White Matter			Gray Matter			Caudate			Putamen			Thalamus		
Sequence	**Fully DESS**	**CS-DESS**	**SPICCS-DESS**	**Fully DESS**	**CS-DESS**	**SPICCS-DESS**	**Fully DESS**	**CS-DESS**	**SPICCS-DESS**	**Fully DESS**	**CS-DESS**	**SPICCS-DESS**	**Fully DESS**	**CS-DESS**	**SPICCS-DESS**
Subject 1	0.1±27.5%	0.7±9.8%	-3.1±10.3%	1.0±33.9%	-0.8±16.0%	-0.8±14.6%	4.4±39.3%	8.8±16.6%	-8.8±16.7%	-2.7±30.9%	2.6±9.9%	2.9±9.2%	1.5±25.0%	3.1±9.2%	-8.4±11.0%
Subject 2	-3.2±46.0%	-1.0±17.9%	0.2±13.3%	-2.6±48.6%	-4.1±19.6%	-3.2±16.6%	-4.0±54.3%	-1.2±24.9%	-4.0±20.1%	3.2±70.4%	-6.1±15.0%	2.0±14.1%	2.3±57.0%	7.6±19.6%	-11.9±12.8%
Subject 3	40.4±38.1%	0.9±15.1%	-3.5±11.7%	14.5±41.7%	2.3±17.3%	-3.5±15.7%	63.6±48.2%	5.3±27.5%	-7.4±17.4%	45.3±30.3%	5.5±10.6%	-7.0±10.5%	63.3±38.8%	-7.0±16.9%	-8.0±11.9%
Subject 4	9.0±34.8%	3.7±15.7%	4.2±12.5%	4.1±38.4%	2.7±17.0%	5.0±15.0%	2.3±51.3%	9.5±21.8%	3.1±15.7%	27.1±34.3%	8.0±12.3%	12.0±10.1%	8.7±39.1%	2.1±11.5%	0.3±11.8%
Subject 5	-24.0±51.8%	0.7±14.6%	1.0±14.4%	-15.5±56.5%	1.2±18.6%	0.5±17.5%	-63.1±64.2%	0.1±20.7%	6.0±17.5%	-31.1±40.0%	6.2±12.5%	7.3±13.9%	-64.7±39.6%	-8.6±14.7%	-2.3±11.9%
Subject 6	17.3±36.3%	-10.6±17.0%	-3.9±11.3%	10.5±42.6%	-15.8±19.0%	-1.0±14.2%	46.7±58.3%	-20.1±25.2%	-11.5±16.3%	41.2±33.4%	-16.8±14.5%	-5.0±9.2%	43.0±32.5%	-11.9±17.6%	2.2±11.5%
Subject 7	8.6±39.1%	8.7±13.2%	6.1±10.0%	2.7±44.7%	3.6±17.2%	5.3±14.3%	34.2±46.2%	11.2±20.2%	8.5±13.8%	17.0±39.7%	12.0±9.6%	5.9±9.9%	34.9±34.1%	17.3±10.4%	2.5±10.7%
Subject 8	17.5±41.3%	10.5±23.9%	5.6±12.4%	7.6±43.0%	8.9±24.7%	5.3±18.9%	30.8±66.4%	11.5±32.0%	4.3±19.6%	34.2±37.4%	15.9±17.7%	12.1±10.9%	27.1±40.7%	1.9±25.1%	2.4±11.7%
Absolute average across all subjects	15.0±13.0%	4.6±4.6%	3.5±2.0%	7.3±5.6%	4.9±5.1%	3.1±2.1%	31.1±25.7%	8.5±6.4%	6.7±2.9%	25.2±16.2%	9.1±5.2%	6.8±3.7%	30.7±25.5%	7.4±5.3%	4.8±4.1%

Table S1: Mean test-retest T_2 differences in all the segmented structures of interest for all subjects. The bottom row shows the average of the absolute mean test-retest T_2 differences across all volunteers.

Supporting Information 4: B_0 Variation and Spoiler effects on the DESS signal and T_2 estimation

Supplementary signal simulations were performed in order to investigate the influence of B_0 variation on the DESS signal as well as the effect of incorporating a spoiler into the sequence. These simulations were achieved via the Extended Phase Graph (EPG) formalism with the Sycomore toolkit[1]. The results of these simulations were then discussed and compared to results from an in vivo experiment.

Simulations n°1 specifics:

As was the case for the simulation of the signal dictionary used for T_2 estimation, the DESS sequence was reproduced by specifying the TEs, TR and flip angle mentioned in "Methods" as well as the unbalanced readout gradient moments. Similarly to Dregely et al[2], an additional spoiler gradient was added in the phase encoding direction in the time separating the two readouts. Its dephasing cycles across a voxel were varied between 0 (i.e., no spoiler) and 20π. A periodic B_0 variation was generated by introducing an offset varying between 0 and 10Hz over a period similar to the respiratory cycle (4 seconds). 10Hz was chosen after considering multiple previous studies recording B_0 variation for brain and breast imaging[3,4]. Simulations were then run for different tissue types, i.e., for combinations of T1[5], T2[6] and ADC[7] values similar to those found in the white matter (WM), gray matter (GM) and cerebral spinal fluid (CSF) regions (Supporting information Figure S3).

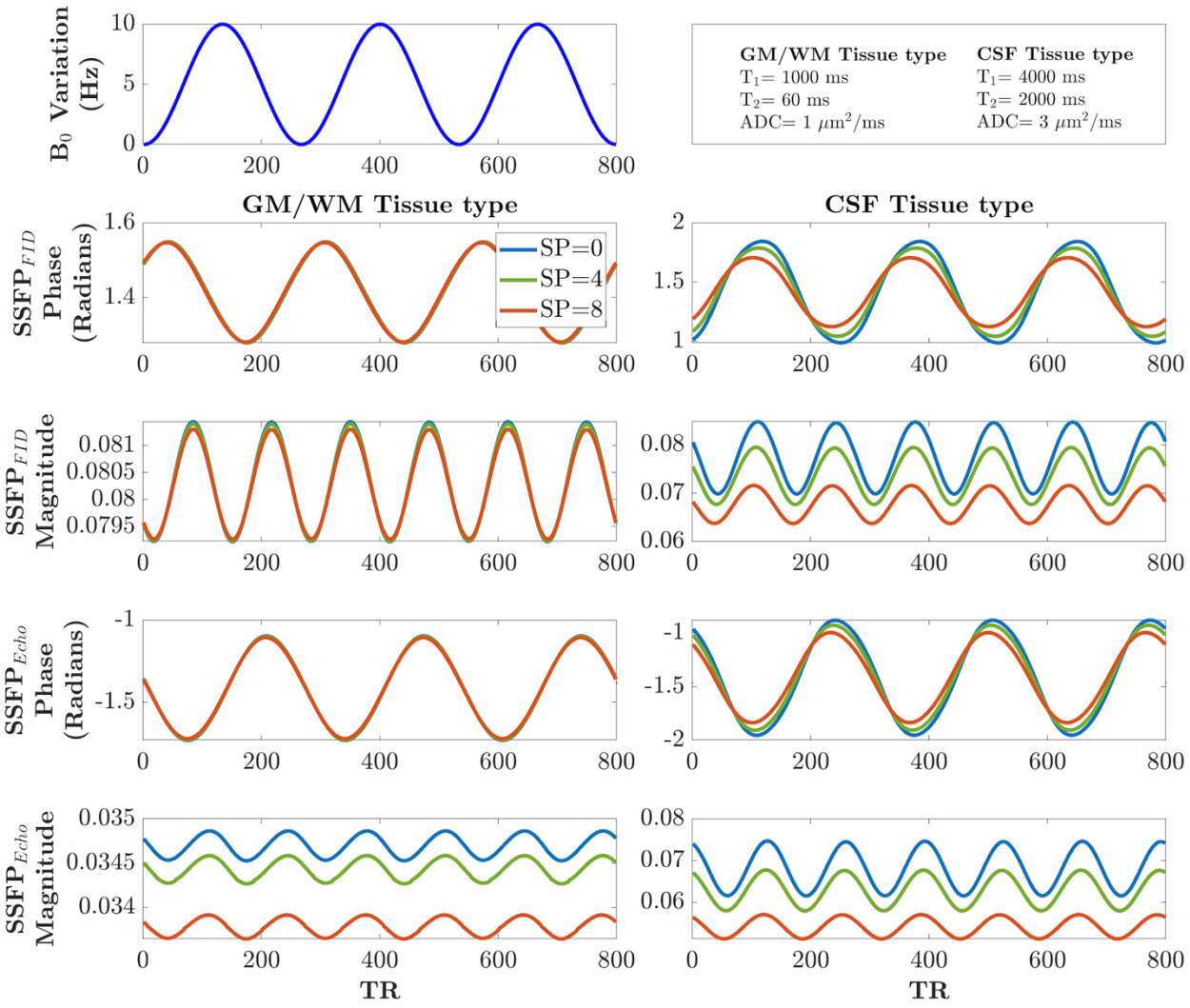

Figure S3: Simulations of a DESS sequence with a periodic 10Hz B_0 variation (top left). The left-hand side depicts the evolution over time of the $SSFP_{FID}$ and $SSFP_{Echo}$ phase and magnitude signals for a gray and white matter tissue type, whereas the right-hand side corresponds to the same evolution for a CSF tissue type (details in the top right). The three different signal curves represent the signals in the cases where the dephasing cycle across a voxel is equal to 2π multiplied by a varying factor SP (0, 4, 8).

Simulations n°1 results:

These simulations demonstrated how a periodic B_0 variation induces a fluctuation in the DESS signals. The phase variations without spoiling were measured to be approximately 0.3 radians and 0.6 radians in the $SSFP_{FID}$ and $SSFP_{Echo}$ respectively for the GM/WM tissue type, and 0.8 radians and 1 radian for the CSF tissue type. These fluctuations followed the same frequency as the respiratory frequency set for the B_0 variation. The magnitude variations were approximately 2.5% and 0.9% of the average signal in the $SSFP_{FID}$ and $SSFP_{Echo}$ respectively for the GM/WM tissue type, and 17% and 16% of the average signal in the CSF tissue type.

The amplitude of these variations was proportional to the B_0 offset (data not shown).

The addition of spoiling demonstrated no notable effects on the DESS signal for the GM/WM tissue type, apart from a slight reduction of the magnitude variations. In fact, if the ADC were set to 0, the spoiler would

have no effect whatsoever regardless of the other parameters (data not shown). On the other hand, the simulation for the CSF tissue type revealed that the strong spoiler gradient (SP=8) could halve the amplitude of the magnitude variations and slightly reduce the phase variations.

Simulations n°2 specifics:

The previous simulations demonstrated that, via the diffusivity of a tissue, a spoiler gradient could have an important effect on signal fluctuations induced by B_0 variation. However, a hypothesized ADC value has to be specified to establish a dictionary signal and subsequently perform a T_2 estimation. The following simulations were thus implemented in order to quantify the error in T2 estimation with respect to the difference between the hypothesized ADC value and the true ADC value. The latter in this case was set to 1 $\mu m^2/ms$. These simulations were done for gray (T1=1300ms, T2=65ms) and white matter (T1=880ms, T2=48ms) tissue types.

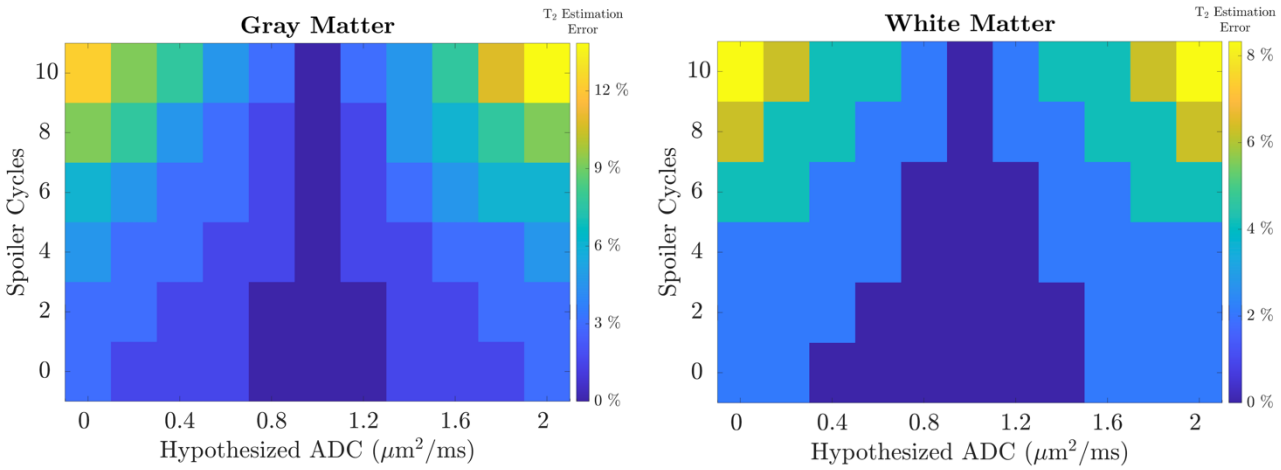

Figure S4: T_2 estimation errors in gray and white matter tissue types with respect to the number of spoiler cycles (SP in Figure S3) and the hypothesized ADC specified for the T_2 estimation (true ADC value here set to 1 $\mu m^2/ms$).

Simulations n°2 results:

This second set of simulations show that without any spoiling, the error in T_2 estimation does not exceed 3% regardless of the hypothesized ADC. However, the more spoiler cycles the more the error increases, reaching up to 12% and 8% in the gray and white matter tissue types respectively, when the difference between the true ADC and the one used in the dictionary is 1 $\mu m^2/ms$.

In vivo experiment:

In order to confirm the results of the previous simulations, an in vivo brain experiment was performed. Two 1.2 mm Fully DESS sequences were acquired on a single subject with the same parameters specified in "Methods", except for a TR set to 20ms to accommodate for an additional spoiler gradient (resulting acquisition time of 8min42s). The only difference between the two acquisitions was the presence of a spoiler

gradient in the second scan and not the first one. This spoiler gradient was set to have an 8π dephasing cycle across a voxel. Three different T_2 maps were then reconstructed for each acquisition, where the ADC used in the dictionary varied from 0 to 2 $\mu m^2/ms$.

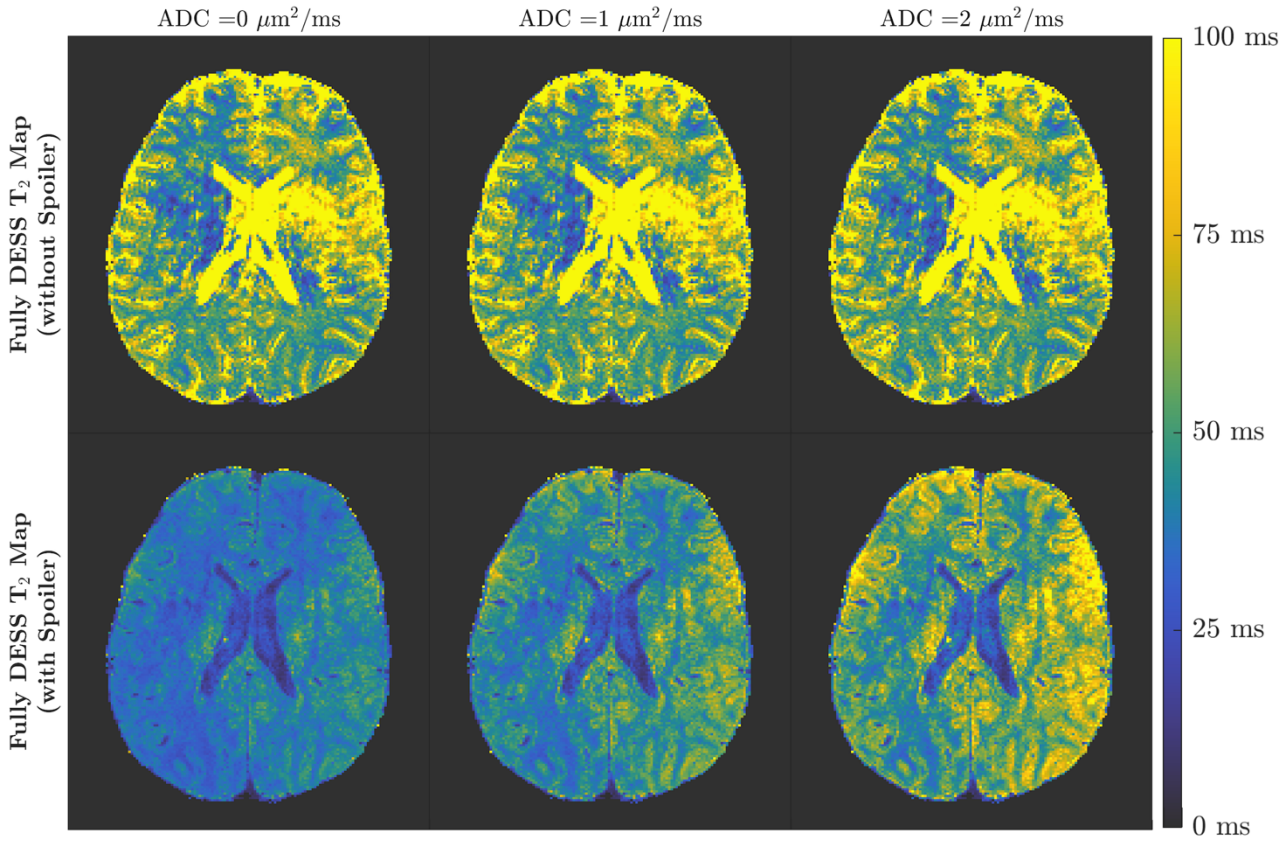

Figure S5: Fully DESS T_2 maps with (bottom row) and without (top row) spoiling. The ADC value used for T_2 estimation is altered from left to right.

<u>In vivo experiment results:</u>

The introduction of a spoiler into the sequence demonstrates a reduction of the ghosting artifact in the brain T_2 maps. This reduction is not complete however, as residual inhomogeneities can be seen in the white matter areas surrounding the ventricles. A stronger spoiler gradient could potentially diminish the artifacts further, but would also lengthen the TR even more. The second important result is the high sensitivity to the ADC specified in the dictionary when the spoiler gradient is played. While the Fully DESS without spoiling has artifacted maps, the T_2 values did not vary much due to a weaker impact of diffusivity. On the other hand, the Fully DESS with spoiling demonstrated a gradual increase in T2 estimates as the specified ADC was varied. This confirms the results obtained in simulations n°2.

<u>Conclusion:</u>

Numerical simulations confirmed that periodic B_0 variations induce both phase and magnitude signal variations. Those variations, notably in the CSF magnitude, can be mitigated by the effect of diffusion, but a large spoiler gradient is needed (meaning a longer TR). By including such a gradient, the ghosting artifact is suppressed in the brain T_2 maps but not completely. Moreover, with such a strong spoiler gradient, a wrong

hypothesis regarding the ADC can induce up to 8-12% errors in the T_2 estimation in the white and gray matter regions, compared to 0-3% errors without the spoiler.

Supporting Information 5: DESS vs Spin Echo T_2 estimation

The following comparison with the gold standard was performed in order to complete this study and measure the accuracy of the different methods.

Phantom and in vivo experiments were conducted in order to compare the DESS sequences to a single slice single shot Spin-Echo EPI sequence. The latter was acquired with the following parameters: TR = 10000 ms, TEs = 17, 22, 27, 37, 47, 57, 77, 97, 117 ms, flip angle = 90°, field of view (FOV) = 160 x 204 x 5 mm^3, matrix size = 80 x 108, GRAPPA factor 4, transversal orientation, A >> P phase encoding direction, bandwidth = 1490 Hz/pixel. The 1.2mm DESS sequences were acquired with the same parameters specified in "Methods". The in vivo brain acquisitions were acquired on a single volunteer whilst the phantom experiments were acquired on 8 tubes immersed in water with the following concentrations:

	Tube 1	**Tube 2**	**Tube 3**	**Tube 4**	**Tube 5**	**Tube 6**	**Tube 7**	**Tube 8**
Agarose gel	5%	7.5%	1.5%	1.5%	1.5%	1.5%	1.5%	1.5%
Gadolinium	0 mM	0 mM	0.3 mM	0.2 mM	0.15 mM	0.05 mM	0.02 mM	0 mM

Table S2: Different Agarose gel and Gadolinium concentrations in the 8 tubes used for the phantom experiments.

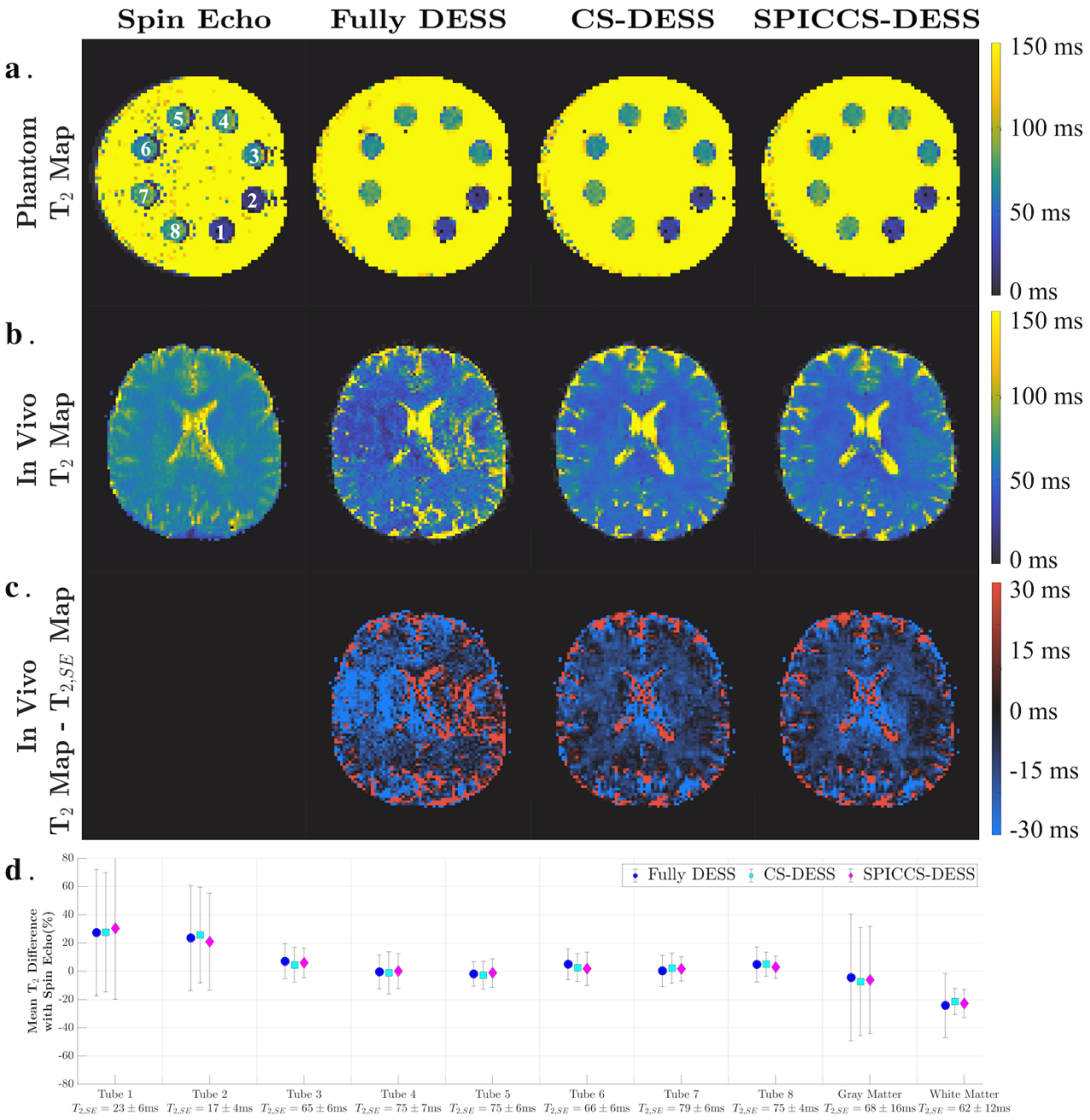

Figure S6: a and b. Phantom and brain T_2 maps reconstructed from the Spin Echo, Fully DESS, CS-DESS and SPICCS-DESS sequences. c. Difference images between the brain Spin Echo (specified as $T_{2,SE}$) and DESS T_2 maps. d. Mean T_2 differences between the Spin Echo and DESS sequences in the 8 tubes as well as the gray and white matter regions.

The resulting maps demonstrated that the DESS sequences provided similar values to the Spin echo sequence in vitro, with T_2 errors below 8% in 6 out of 8 tubes. Given the particularly short T_2 values of both remaining vials (~20ms), their relative error reached 30% but the absolute differences remained below 5ms. However, the DESS sequences underestimated the T_2 values in the gray and especially the white matter, compared to the spin-echo sequence. As the differences are much less notable in the phantom experiments, this suggests that some phenomenon that is not accounted for in the DESS methods, such as magnetization transfer for instance, could potentially induce this offset in T_2 values.

1. Lamy J, de Sousa PL. Sycomore: an MRI simulation toolkit. *Proc Intl Soc Mag Reson Med 28*. 2020:1038.
2. Dregely I, Margolis DAJ, Sung K, et al. Rapid quantitative T2 mapping of the prostate using three-dimensional dual echo steady state MRI at 3T. *Magn Reson Med*. 2016;76(6):1720-1729. doi:https://doi.org/10.1002/mrm.26053
3. Moran CJ, Granlund KL, Sveinsson B, Alley MT, Daniel BL, Hargreaves BA. Respiration Induced B0 Variation in Double Echo Steady State Imaging (DESS) in the Breast. *Proc Intl Soc Mag Reson Med 23*. 2015:498.
4. Van de Moortele PF, Pfeuffer J, Glover GH, Ugurbil K, Hu X. Respiration-induced B0 fluctuations and their spatial distribution in the human brain at 7 Tesla. *Magn Reson Med*. 2002;47(5):888-895. doi:10.1002/mrm.10145
5. Bojorquez JZ, Bricq S, Acquitter C, Brunotte F, Walker PM, Lalande A. What are normal relaxation times of tissues at 3 T? *Magn Reson Imaging*. 2017;35:69-80. doi:10.1016/j.mri.2016.08.021
6. Spijkerman JM, Petersen ET, Hendrikse J, Luijten P, Zwanenburg JJM. T2 mapping of cerebrospinal fluid: 3 T versus 7 T. *Magma N Y N*. 2018;31(3):415-424. doi:10.1007/s10334-017-0659-3
7. ELLINGSON BM, KIM E, WOODWORTH DC, et al. Diffusion MRI quality control and functional diffusion map results in ACRIN 6677/RTOG 0625: A multicenter, randomized, phase II trial of bevacizumab and chemotherapy in recurrent glioblastoma. *Int J Oncol*. 2015;46(5):1883-1892. doi:10.3892/ijo.2015.2891